The PHENIX Forward Spectrometer Upgrade

(selected sections from the PHENIX forward upgrade letter of intent)

Brookhaven National Laboratory
Edward Kistenev, Pete Kroon, Mike Tannenbaum, Craig Woody

University of Colorado
Frank Ellinghaus, Ed Kinney, Jamie Nagle, Joseph Seele, Matt Wysocki

University of California at Riverside
Ken Barish, Stefan Bathe, Tim Hester, Xinhua Li, Astrid Morreale, Richard Seto, Alexander Solin

University of Illinois at Urbana Champaign
Mickey Chiu, Matthias Grosse Perdekamp, Hiro Hiejima, Alexander Linden-Levy Cody McCain, Jen-Chieh Peng, Joshua Rubin, Ralf Seidel

Iowa State University
John Lajoie, John Hill, Gary Sleege

Kyoto University
Kazuya Aoki, Ken-ichi Imai, Naohito Saito, Kohei Shoji

Moscow State University
Mikhail Merkin, Alexander Voronin

Nevis Laboratory
Cheng Yi Chi

University of New Mexico
Doug Fields

RIKEN
Atsushi Taketani

RBRC
Gerry Bunce, Wei Xie

University of Tennesee
Vasily Dzhordzhadze, Ken Read

Table of Contents

Executive Summary 3

1. Proposed Scientific Program 5
   1.1 Overview
   1.2 p-A Physics
      1.2.1 Gluon Saturation and Shadowing 6
      1.2.2 Quark Shadowing and P_T Distributions 7
      1.2.3 Detector Requirements for the Upgrade 8
   1.3 A-A Physics 9
      1.3.1 Quarkonia Physics in Nuclear Collisions
         1.3.2 Extending Measurement of Quarkonia with the NCC 11
         1.3.3 Photon-Jet Physics with the NCC 12
   1.4 p-p Physics 14

2. Design Considerations for the new Forward Detectors 19
   2.1 Overview
   2.2 Muon Trigger Upgrade
      2.2.1 Motivation: Decay Muons and Beam Background
         2.2.2 Performance of the present Muon Trigger 20
         2.2.3 Muon Trigger Upgrade with RPCs 21
         2.2.4 Upgrade with a new MuTr FEE 22
      2.2.5 R&D for new MuTr FEE 24
      2.2.6 RPC R&D 25
      2.2.7 Front End Electronics 26
   2.3 Nosecone Calorimeter (NCC)
      2.3.1 Conceptional Design
      2.3.2 Detector Layout and Configuration 27
      2.3.3 Event Environment in NCCs 3 3
      2.3.4 Effect of NCC on Muon Measurements 35
      2.3.5 FEE (Readout, Signal Packaging and Processing) 36
   2.4 Local Level-1 Trigger Electronics 38
      2.4.1 The NCC Level-1 Trigger System 40

3. Collaboration 42

Cost and Schedule 43
   4.1 Sources of Funding
   4.2 Schedule 44

Executive Summary

We are proposing a significant upgrade of the PHENIX muon detector systems which will dramatically extend the detection capabilities and physics reach of the existing PHENIX forward muon spectrometers. The forward upgrade of the PHENIX detector as described in this document consists of two main components:

(1) The addition of two large acceptance W-Si sampling calorimeters, $0.9<|\eta|<3.0$ with full azimuthal coverage, which will replace the present nosecone absorbers. The new nosecone calorimeters will be located upstream of the present PHENIX muon spectrometer arms and will provide neutral pion, photon and jet detection.

(2) The insertion of dedicated first level trigger detectors in the muon spectrometer. These will provide level one triggering in the PHENIX muon arms at the highest luminosities anticipated for future polarized proton running and possibly a first level trigger for quarkonium physics in heavy ion collisions at RHIC II luminosities.

In combination these upgrades will enable PHENIX to carry out a broad range of new and unique measurements:

> *W*-production in polarized proton-proton collisions at $\sqrt{s}$=500 GeV with a luminosity of $L=10^{32}cm^{-2}s^{-1}$ will lead to a theoretically clean measurement of flavor-separated quark and anti-quark polarizations $\Delta q/q$ in the proton. The measurement of quark polarizations in W-production will be free of the large uncertainties connected with the low scales in semi inclusive deep inelastic measurements and the poor knowledge of fragmentation functions.
>
> Studies of the modification of nucleon structure in the nuclear environment in proton-ion or deuteron-ion collisions will make it possible to search for new states of matter at high parton densities as for example the "color glass condensate" (CGC) and the "color quantum fluid" (CQF).
>
> In heavy ion collisions the upgrades aim at a survey of bottomonium bound states and the measurement of additional charmonium states such as the χ_c which cannot be accessed with the detectors presently available at RHIC. The observation of quarkonium formation with a broad range of different binding energies will provide a measurement of the temperature and the dynamics of the dense nuclear medium formed in heavy ion collisions at RHIC. We are presently studying the possibility to use the nosecone calorimeter for jet-photon physics in heavy ion physics thus significantly extending the limited acceptance of the PHENIX central spectrometers in this physics channel.

At this time we have not evaluated possible synergy or overlap with the existing forward silicon upgrade project. We have initiated the necessary discussions and will provide an

evaluation of possible integrated forward upgrade solutions in the near future. A day long meeting on PHENIX forward upgrades has been scheduled as part of the PHENIX muon collaboration meeting in Santa Fe, June 21- 23.

Among PHENIX institutions collaborators from twelve groups have joined the forward upgrade activities: BNL, Kyoto, RIKEN, RBRC, MSU, UCR, Nevis, UNM, ISU, Colorado, UIUC and Tennessee. The group from Moscow State University has recently joined PHENIX with the explicit interest of collaborating on the proposed forward upgrade. We are actively pursuing additional groups and have an expression of interest from an INFN group in Trieste and continuous contact with a group at the INFN in Frascati.

It is our goal to formally propose the muon trigger section of the PHENIX forward upgrade to the National Science Foundation for support in January 2005. We seek funding from DOE and foreign sources for the nosecone calorimeters.

1. Proposed Scientific Program

1.1 Overview

The Relativistic Heavy Ion Collider is the premier facility for the experimental study of the strong nuclear force as illustrated by it's extraordinary scientific breadth : RHIC was originally conceived for the study of strong interaction phenomena at the highest accessible energy densities in heavy ion collisions. RHIC succeeds extensive heavy ion physics programs at the AGS at BNL and the SPS at CERN and increases the accessible energy scale by one order of magnitude.

The advent of modern QCD re-summation techniques and the development of high energy polarized proton beams in RHIC have made it possible to extend the physics program at RHIC with an ambitious plan to explore the origin of the proton spin. The study of proton spin structure in polarized proton collisions at high energies builds on and competes with experiments to study nucleon structure in deep inelastic scattering at SLAC, CERN, DESY and Jefferson Laboratory with unique capabilities to access polarized gluon, quark and anti-quark distributions in the proton.

Proton-ion or deuteron-ion collisions at RHIC make it possible to study nucleon structure as function of their nuclear environment at energy densities at least a factor five higher than at previous experiments at FNAL or CERN. Forward production of inclusive hadrons, jets, direct photons or Drell-Yan pairs at small x_{ion} in nucleon-ion collisions at RHIC will provide a new window for the observation of saturation phenomena expected at high parton number densities. In particular it may be possible to confirm or falsify the existence of the color glass condensate at high gluon densities prior to the arrival of e-A collisions at HERA or e-RHIC.

The proposed upgrade will greatly enhance or introduce new detection capabilities of the PHENIX detector in forward direction including high momentum single muons, neutral pions, jets and single photons. This will lead to a broad physics program adding exciting new physics channels to the heavy ion and spin physics program at RHIC and pioneering the exploration of nuclear effects on the gluon distribution function in the

1.2 p-A Physics

Recently there has been an enormous interest in high energy collisions with nuclei. McLerran and his colleagues have proposed that the initial conditions in heavy ion collisions could be calculated assuming that the gluon distributions at low x are saturated. This is closely related to nuclear shadowing – that is the reduction of the interaction cross section of lepton-nuclear scattering as compared to the incoherent sum of interaction cross sections at high energies or equivalently small x. In fact the Gluon saturation calculations may be a way to understand the phenomenon of shadowing in a rigorous and calculable way. Whether or not the saturation model is shown to be ultimately the correct

description of the low-x gluon structure functions at RHIC, it is important to understand nuclear structure functions in their own right. In general proton nucleus collisions at high energies will enable us to measure quark and gluon distributions in nuclei and will allow a test of whether saturation pictures such as the well known Colored Glass Condensate are correct and the extent to which it gives an approach to calculating shadowing consistent with other methods. Proton nucleus collisions will also allow measurements of anti-quark distributions at low-x as well via di-lepton (Drell-Yan) production.

A variety of probes can be used to examine quark and gluon distributions at low x: direct photon production is a particularly attractive channel to probe the gluon distributions. Heavy quark and J/ψ production, also sensitive to gluon distributions can be measured via high momentum leptons. A probe for the gluon distribution which can be used at lower luminosity, which is being exploited to great advantage for the spin measurements, is inclusive π^0 production. Recently we have gained enormous confidence in NLO calculations of this process when a first measurement was made comparing the calculations to data [1].

1.2.1 Gluon Saturation and Shadowing

In the Colored Glass Condensate (CGC) picture, the gluon distributions at low-x for protons $\sim 1/x^{\delta}$ violate unitarity at very low x and saturate. In protons this should occur at about $x \sim 10^{-4}$-10^{-5} depending on the Q^2. In a Lorentz contracted nucleus, however, there is essentially a geometric enhancement factor of $A^{1/3}$ making the relevant $x \sim 10^{-2}$-10^{-3}. McLerran and his colleagues assume that since the occupation numbers were high, one could use a classical approximation. This allows them to do non-perturbative calculations of various experimentally measured quantities, using renormalization group methods, which depend on the scale Q_s, the saturation momentum, which is around 1-2 GeV/c at RHIC energies. One key to this calculation is that the Q^2 must be greater than about 1 GeV^2 so that the coupling constant is reasonably small ~0.3 [2].

On the experimental side, saturation is a property of the initial state of a proton or nucleus and hence can be probed using proton-nucleus collisions. One would like to measure the gluon distribution functions at very low x to directly observe the saturation. This can be done using a variety of probes as mentioned previously – One key ingredient must be access to the low -x region which typically means that one must measure at forward and backward rapidities at RHIC energies.

A simple diagram of the CGC region and its associated region, the Colored Quantum Fluid (CQF), is shown in figure 1.2.1. Recent results [3] from all of the RHIC detectors in dA collisions have placed high p_T collisions at central rapidity at RHIC outside these regions, so there is no suppression of high p_T particles in the central region in dA collisions. Multiplicity distributions in Au-Au collisions, however, dominated by low momentum particles, appear to be within the region. This is indicated by the lowest red line in the figure which gives strength to the argument that at high p_T, in Au-Au collisions at RHIC, the suppression of hadrons comes not from saturation effects in the initial state, but rather from energy loss in the final state such as jet quenching. Early data from dA collisions at higher rapidities, however, indicate that high momentum particles are suppressed indicating that RHIC may be in the CQF region. It becomes important therefore to explore the region between x of 10^{-2} and 10^{-3} to map out the boundaries

between various regions. This can be done by looking at R_{dA} via the measurement of hadrons (in the case of the nosecone calorimeter by measuring π^0's), then exploring shadowing effects via the measurement of the gluon structure function via the study of direct photons and open charm/bottom.

1.2.2 Quark Shadowing and p_T Distributions

The CGC is of course not the only framework in which shadowing or other related low-x phenomena have been considered. The phenomenon of nuclear shadowing which is the reduction of the interaction cross section for lepton-nucleus scattering compared to the incoherent sum of the individual cross sections at high energies (small x) has a long history. For a recent review and references see [4]. Shadowing in this picture is due to a large coherence length for interactions at small x. Several experimental groups observed the phenomena in studies of deep inelastic muon-nucleus scattering. There is evidence of small nuclear shadowing for the lowest x=0.03 data point of the FNAL Drell-Yan data [6].

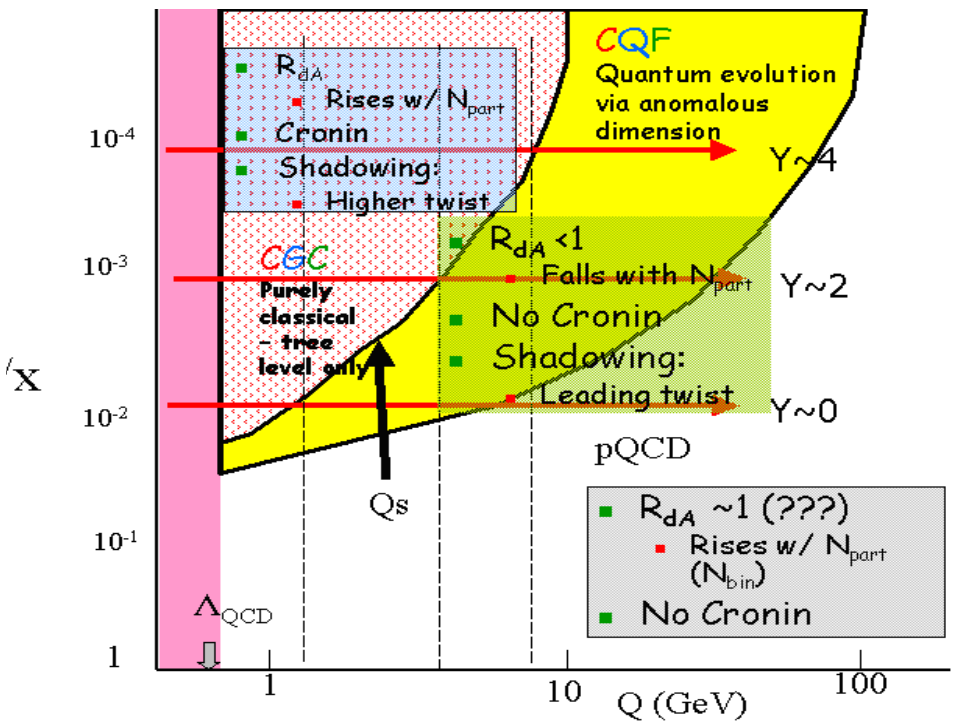

Figure 1.2.1 CGC diagram.

The major obstacle that hinders our deeper knowledge of nuclear parton distribution functions (nPDFs) at small x is that, up to the present day, all experiments aiming to study nPDFs are performed with fixed nuclear targets. In these data, the values of x and Q^2 are strongly correlated and one measures nPDFs essentially along a curve in the x-Q^2 plane rather than exploring the entire plane. Moreover, for $Q^2 > 1$ GeV^2, the data cover the region $x > 5\times10^{-3}$, where the effect of nuclear shadowing is just setting in.

1.2.3 Detector Requirements for the Upgrade

The primary goals of this upgrade will be the measurement of the gluon structure functions at low x down to 10^{-3} at Q^2 between 1 and 100 GeV^2. From this we derive the following performance goals for the PHENIX forward upgrades:

1) measurement of photons, neutral pions and jets to rapidities of $\eta \sim 3.0$ giving a coverage for x_2 down to 10^{-3}.
2) the separation of photons and π^0's in this region.
3) the reconstruction of jet direction, and a very crude energy measurement.
4) the detection of muons at the highest rates consistent with the luminosities planned for RHIC II.

In combination, the new calorimeter and the muon trigger upgrade will provide access to the physics processes listed in the introduction and thus provide access to the gluon distribution in nuclei at small x. It will be important to measure all processes in both pp and pA (or dA) since we seek to identify effects that are unique to nuclei.

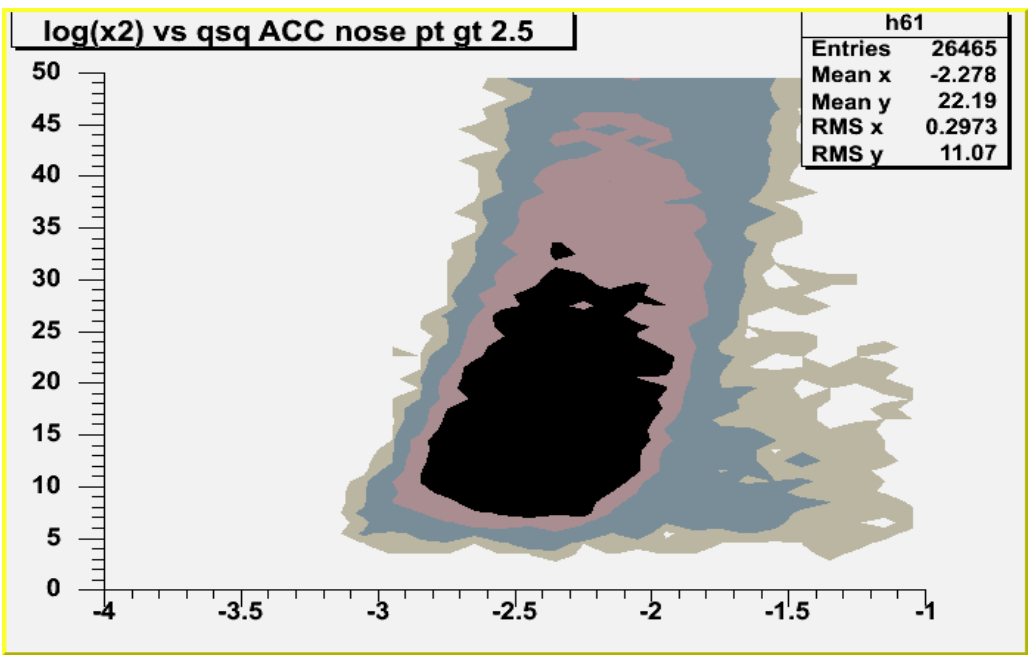

Figure 1.2.2 Coverage of NCC for direct photon events in 100x100 GeV^2 pA collisions.. The x-axis corresponds to $\log(x_2)$, the y-axis to Q^2 in GeV^2. The contours correspond to the number of events in bins of 0.1 in $\log(x_2)$, and $1GeV^2$ in Q^2. The contours are 20 events/bin, 20 events/bin, 100 events/bin, 500 events/bin and 1000 events/bin. .

We use an event generator study with PYTHIA in order to obtain a better estimate of the kinematic range covered with the proposed NCC. This study looked at direct photon events from phythia, as an example of what might be done. The photon is required to have a minimum transverse momentum of 2.5 GeV and to be in the pseudo rapidity

interval between 0.9 and 3. The results are shown in figure 1.2.2. The plot corresponds to a 0.5 pb^{-1} pAu run, as planned in run 12 of the PHENIX beam use proposal. There are 4 contours shown which correspond to the number of events in a bin of $\log(x_2)$ and Q^2 of 0.1 x $1GeV^2$. The numerical values for the contrours from ouside in are 20 events per bin, 100 events/bin, 500 events/bin, and 1000 events/bin.

References:

[1] S.S. Adler et al. [PHENIX Collaboration], Phys. Rev. Lett. 91, 241803 (2003).
[2] L. D. McLerran and R. Venugopalan, Phys. Rev. D 49, 3352 (1994)[arXiv:hep-ph/9311205].
[3] S.S. Adler et al. [PHENIX Collaboration], Phys. Rev. Lett. 91, 072303 (2003); I. Arsene et al [BRAHMS Collaboration], arXiv:nucl-ex/0403005; M. Liu [PHENIX Collaboration] arXiv:nucl-ex/0403047.
[4] G. Piller and W. Weise, Phys. Rept. 330, 1 (2000)[arXiv:hep-ph/9908230].
[5] L. Frankfurt and M. Strikman, Phys. Rev. Lett. 91, 022301 (2003) [arXiv:nucl-th/0212094].
[6] P. L. McGaughey, J. M. Moss and J. C. Peng, Ann. Rev. Nucl. Part. Sci. 49, 217 (1999)[arXiv:hep-ph/9905409].
[7] R. Baier, D. Schiff and B. G. Zakharov, Ann. Rev. Nucl. Part. Sci. 50 (2000) 37 [arXiv:hep-ph/0002198].

1.3 A-A Physics

1.3.1 Quarkonia Physics in Nuclear Collisions

A principal design consideration of the PHENIX muon spectrometer was the ability to identify and reconstruct heavy quarkonia via their decay to muons. The production of quarkonia in nuclear collisions is of fundamental importance to the experimental nuclear physics program at RHIC because these states are sensitive to both the gluon distribution of the initial state nuclear wave function and by virtue of their relatively long formation time to the ensuing dense partonic media. The formation time of the precursor heavy quark pair is given by the heavy quark mass and is $O(1/m_c \sim 0.1fm)$. In order to form a bound state the precursor state grows to the size of the physical quarkonia over a time scale given by relative momentum of the heavy quarks in the bound state $O(1/m_c \sim 1\ fm)$. During the evolution of the precursor the surrounding nuclear medium can influence the formation of the bound state quarkonia by color screening the attractive potential between the heavy quarks [1], thus leading to the suppression of the formation of heavy quarkonia and nuclear induced reactions.

Since quarkonia production was first proffered as an experimental observable sensitive to the presence of a deconfined partonic phase (Quark Gluon Plasma) there have been efforts of ever increasing sophistication to calculate the temperature dependence of the

dissolution of heavy quark bound states using finite temperature QCD on the lattice. Fig. 1.3.1 shows the screening radius from the lattice versus temperature and the radii of 1S, 2S and 1P quarkonia. In contrast to earlier results based upon modifications to the heavy quark potential which predicted the J/ψ to melt at around the critical temperature for transition to a QGP [2], current predictions indicate the J/ψ persists until 2.5 times the critical temperature and the more deeply bound Upsilon (1S) will persist to temperatures well beyond that.

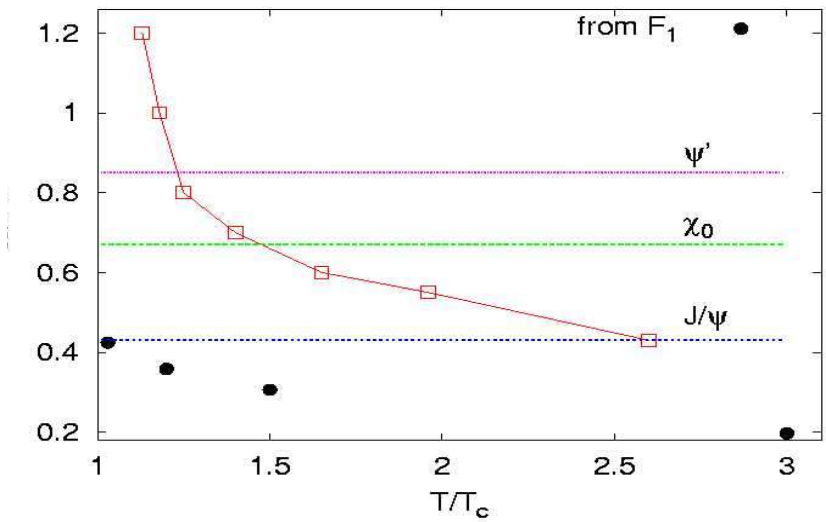

Figure 1.3.1 Screening radius from lattice calculations and the radius of 1S, 2S, and 1P quarkonia.

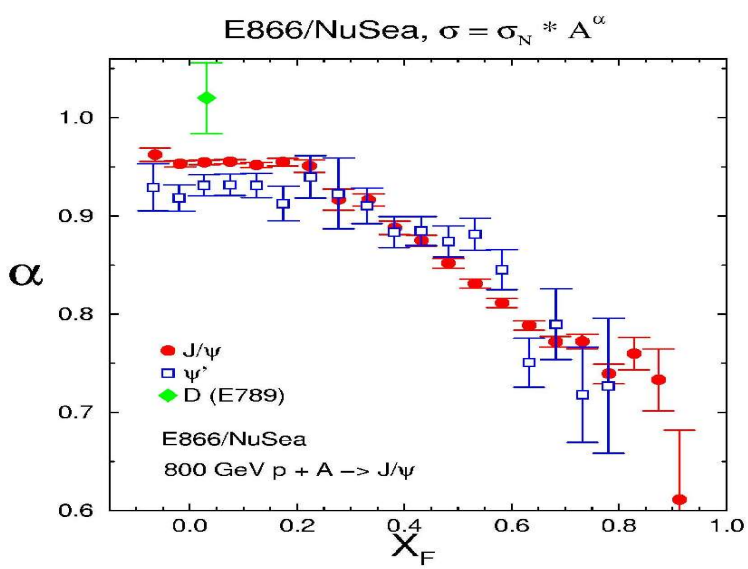

Figure 1.3.2 x_F dependence of suppression of scaling as measured by E866 at Fermilab

1.3.2 Extending Measurement of Quarkonia with NCC

As is the case with most other experimental probes of the dense partonic system produced in the aftermath of a heavy ion collision at RHIC the suppression of the production of quarkonia can plausibly be attributed to nuclear effects other than the proposed suppression by dynamic color screening from a hot deconfined plasma of quarks and gluons. The most straightforward method by which competing effects can be made less ambiguous is to measure as many of the quarkonia states as is possible. This idea is not without precedent, figure 1.3.2 shows the x_F dependence of suppression of scaling as measured by E866 at Fermilab. [3] At moderate values of x_F the difference between the suppression of 1S and 2S quarkonia is indicative of different nuclear absorption cross sections in accordance with the expectations based upon the factor of 2 difference in the size of the bound states. [4] As is the case with precursor absorption in cold nuclear matter the ability to measure multiple quarkonia states and connect the observed suppression pattern with theory will be of great benefit in unambiguously attributing an observed suppression pattern to the formation of a deconfined medium.

The proposed nosecone electromagnetic calorimeter (NEMC) has the potential to extend the measurement of quarkonia at RHIC to include P wave quarkonia χ_c states via their radiative decay $\chi_c \rightarrow \gamma\ J/\psi$. The χ_{c1} and χ_{c2} states are produced with cross sections commensurate with that of the J/ψ and their radiative decay channels have appreciable branching fractions (0.27 and 0.17 respectively). The measurement of χ_{c0} is precluded by its radiative decay small branching fraction (~ 0.01). The PHENIX muon spectrometer has pseudorapidity coverage $1.2 < |\eta| < 2.2$ (2.4) in the south (north) muon arms respectively. The photon from the radiative decay of χ_c has a small relative momentum to that of its parent and therefore the proposed NEMC has good acceptance (58%) for γ associated with J/ψ that are in the acceptance of the muon spectrometer.

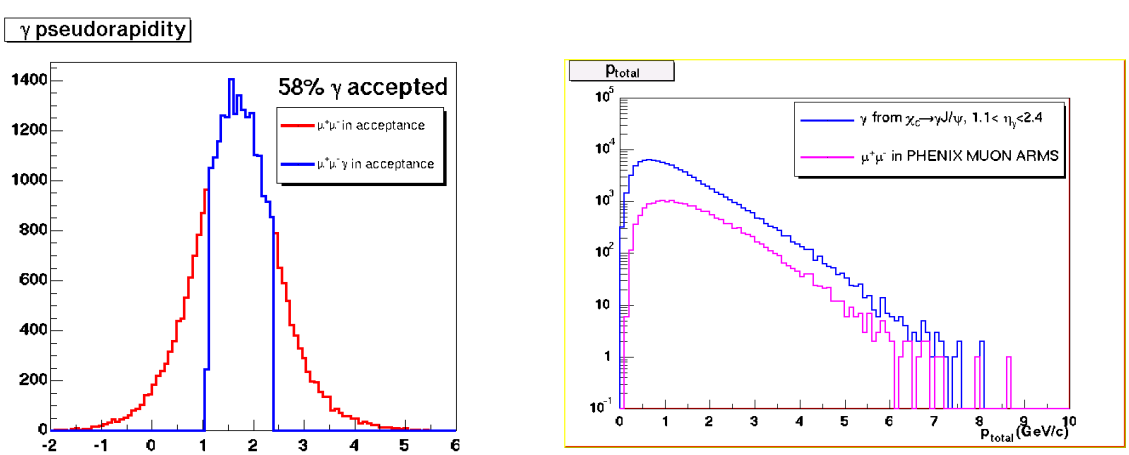

Figure 1.3.3 (Left) The acceptance of γ associated with an accepted J/ψ t and (Right) The total momentum of accepted γ.

Figure 1.3.3 shows the acceptance of γ associated with an accepted J/ψ and the total momentum of accepted γ. The resolution for J/ψ in the current PHENIX muon spectrometer is limited by multiple-scattering and energy loss fluctuations in the hadronic absorber that exists between the spectrometer and the primary collision. It has been shown with a fast Monte-Carlo that the resolution of the reconstruction of χ_c for any reasonable range of calorimeter energy resolution is dominated by the angular resolution of the reconstructed J/ψ. Figure 1.3.4 shows the invariant mass distribution of reconstructed χ_c with 2 different scenarios for the energy resolution of the NEMC and momentum resolution in the muon spectrometer commensurate with the observed J/ψ resolution from Run III data at RHIC.

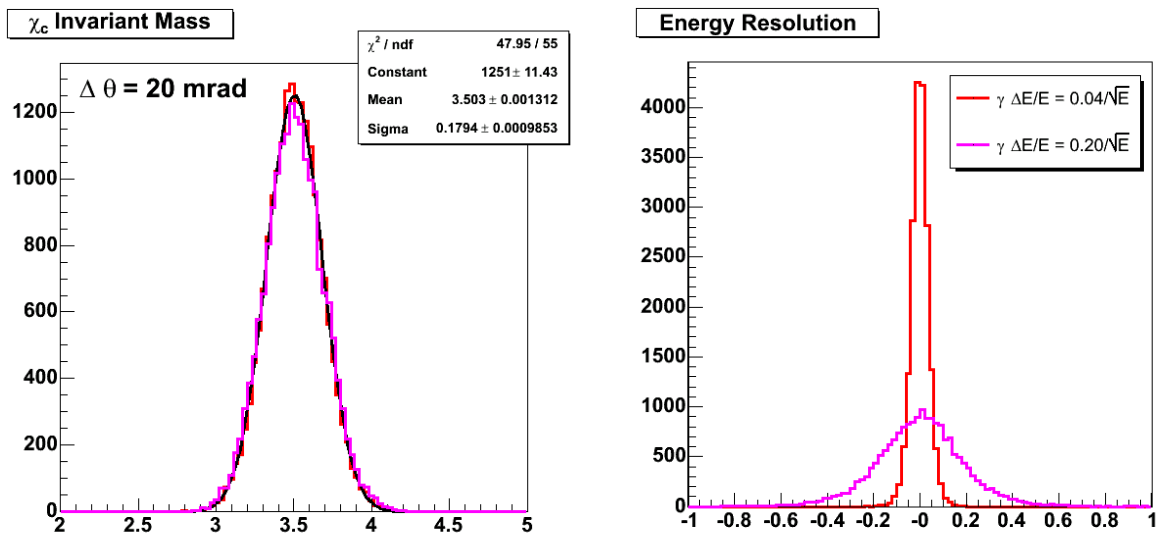

Figure 1.3.4 (Left) The invariant mass distribution of reconstructed χ_c with 2 different scenarios for the energy resolution of the NEMC (Right) and momentum resolution in the muon spectrometer.

The 170 MeV resolution determined by this simulation could be significantly improved with additional measurements by the muon spectrometer of the upstream muon trajectory and the use of a 3 body kinematic fit.

1.3.3 Photon-Jet Physics with the Nosecone Calorimeters

We are presently in the process of studying the utility of the proposed nosecone calorimeter for photon-jet physics in heavy ion collisions. The principal problem is to understand the possibility of identifying jet fragments among the background from the underlying event in heavy ion collisions. At RHIC energies this question will depend sensitively on the collision systems and centrality.

References

[1]T. Matsui and H. Satz, Phys. Lett. B **178**, 416 (1986).
[2] Kharzeev & Satz, P.Petresky QWG
[3] M.J. Leitch *et al*., Phys. Rev. Lett. **84**, 3256
[4] B.Kopeliovich

1.4 p-p Physics

A central goal of high-energy nuclear physics is to determine and understand the quark-gluon structure of the nucleon, the fundamental bound state of QCD. The present understanding is largely empirical and rudimentary. A prime example of this is the surprising fact, now well established from inclusive polarized deep inelastic lepton scattering experiments, that only 20-30% of the spin of the nucleon arises from the spins of the quarks. While one would expect a significant contribution from the gluon field, this contribution remains almost completely undetermined. Possible contributions from orbital angular momentum are even less well understood, both experimentally and theoretically, although there are recent hints that this contribution is not small.

The PHENIX experiment, along with the STAR and COMPASS experiments, will make the first direct measurements of the gluon contribution to the nucleon spin, $\Delta G(x)$, over a significant range in momentum fraction x. The basic processes are polarized gluon-gluon and polarized quark-gluon hard scattering leading to different final states, as shown in Fig. 1.4.1.

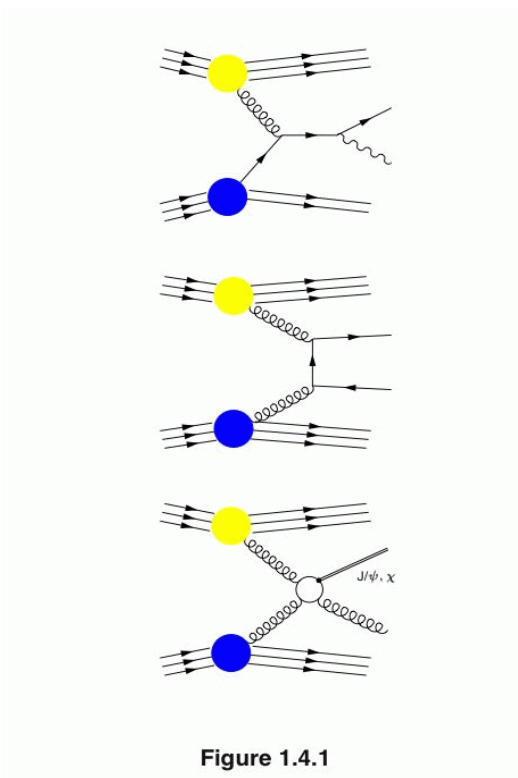

Figure 1.4.1 Basic processes sensitive to the gluon polarization.

First results from PHENIX Run 3 have already been produced which constrain models with different gluonic spin contributions. With future data acquisition, the variety and power of these measurements will greatly increase.

Given these measurements, a fundamental question will be how the quark and gluon contributions mutually arise in the nucleon bound state. In particular, how is the polarization of the sea quarks, which are formed from the gluon field, affected by the polarization of this field. In order to answer this more detailed question, experiments at CERN (SMC, COMPASS) and DESY (HERMES) have and are attempting to determined the spin contributions of the different quark flavors separately, especially the contri-butions from the sea quarks. The technique used is so-called "hadron tagging" based on the measurement of semi-inclusive asymmetries, in which a leading hadron (*i.e.,* a hadron containing a large fraction of the energy transferred to the nucleon) is detected in coincidence with a deep-inelastically scattered lepton. Using statistical analysis and empirical fragmentation models, one can exploit the greater than random probability that the leading hadron contains the struck quark, and use the hadron species to limit the possible

flavor of the struck quark. Measuring concurrently a sufficient number of semi-inclusive asymmetries with identified leading pions and kaons allows an extraction of the spin contributions from the different quark and anti-quark (sea) flavors. The results of the analysis of the HERMES data are shown in Fig. 1.4.2.

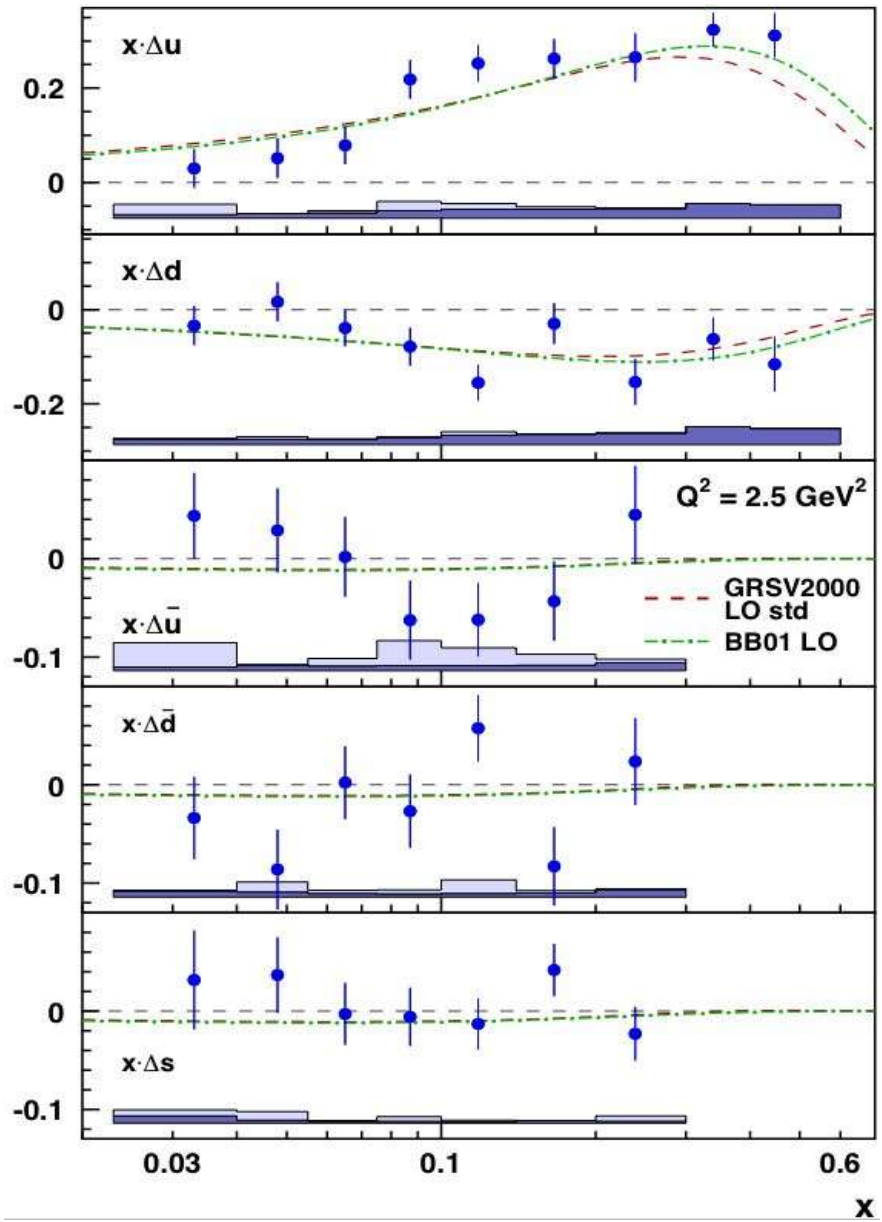

Figure 1.4.2 Results of HERMES spin-flavor decomposition using semi-inclusive deep-inelastic electron scattering *(A. Airapetian et al., Phys. Rev. Lett. 92 (2004) 012005)*.

To date, this extraction has only been performed within a leading order (LO) QCD "framework", that is, with the effects of the Q^2 evolution only minimally included and no attempt at inclusion of higher twist effects. Several theoretical programs to extend the

semi-inclusive analysis procedure to next-to-leading order (NLO) are underway. A chief concern with the HERMES analysis is the relatively low Q^2 (average about 2.5 GeV^2) of the data, which may result in large NLO corrections. The forthcoming analysis from COMPASS will certainly use a data sample with significantly higher Q^2 which will likely have smaller NLO corrections. Furthermore, it will extend the determination to almost an order of magnitude smaller x value than HERMES. Because COMPASS only will use a polarized deuterium target, some additional assumptions about the proton and neutron parton distributions will be required. Nonetheless, the HERA collider experiments have shown just how strongly coupled the resolution of the sea distributions are to the Q^2 of the probe, so it remains important to measure the spin-flavor composition of the nucleon up to the highest Q^2 possible.

However, a common systematic uncertainty in the analysis of both experiments is the hadron-tagging technique itself, which relies on the use of fragmentation function models which in some cases (*e.g.,* s quark fragmentation to kaons) are not well known due to a general lack of data, especially at lower energies. While there is hope that new (and voluminous) data from the Belle experiment will significantly improve this situation, there will remain issues related to possible differences in how the fragmentation process occurs starting from the initial quark-antiquark pair in e+e- colliders and the process starting from a quark struck from a nucleon. Furthermore, both COMPASS and HERMES suffer from the "u-quark dominance" caused by the weighting of the fundamental photon-quark interaction by the square of the quark charge. Hence it is difficult to extract precise information about the down and strange quark (and anti-quark) polarized distributions. Since the weak interaction lacks this bias, intense high energy neutrino beams would be ideal for this type of semi-inclusive analysis.

Fig. 1.4.3 $W^{+/-}$ production in polarized pp scattering.

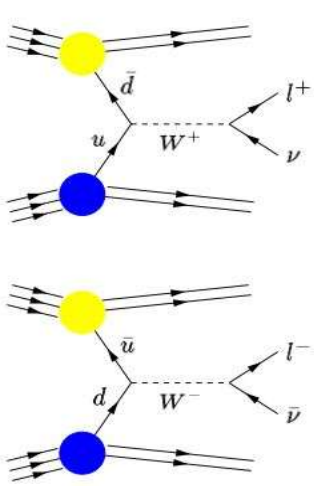

Figure 1.4.3

The collision of high-energy polarized protons at RHIC provides a completely new means to use the weak interaction as a probe of the polarized parton distributions, namely $W^{\pm}$ production, leading to a very high energy muon or electron, of the same charge as the W and with an energy of roughly half the W mass, as shown in Fig 1.4.3. This measurement and estimates of the sensitivity are described thoroughly in Refs. [1], [2], and [3], so we here recall the major points. This reaction mechanism offers a number of advantages over deep-inelastic scattering: there are no systematic uncertainties from fragmen-tation models, there is no u-quark dominance arising from the intrinsic vertex coupling strength, the parity violating nature of the weak interaction provides a natural polarization measurement so that only a single spin asymmetry is required, and the Q^2 of the measurement is very high, essentially at the mass squared of the W boson.

Figure 1.4.4 shows the results of a simulation of the expected statistical accuracy of a measurement for 800 pb^{-1} integrated luminosity, 70% beam polarization, and with the PHENIX detector assuming the nominal energy and solid angle acceptance. However, it assumes that the rapidity of the W can be determined accurately, whereas in fact, because the neutrino is not detected, one can only determine the decay charged lepton's rapidity and p_T, and then via a statistical analysis relate the rapidity and p_T asymmetries to those of the parent W bosons. These effects and also higher order QCD corrections have been extensively investigated by Nadolsky and Yuan in Reference [1.4.3].

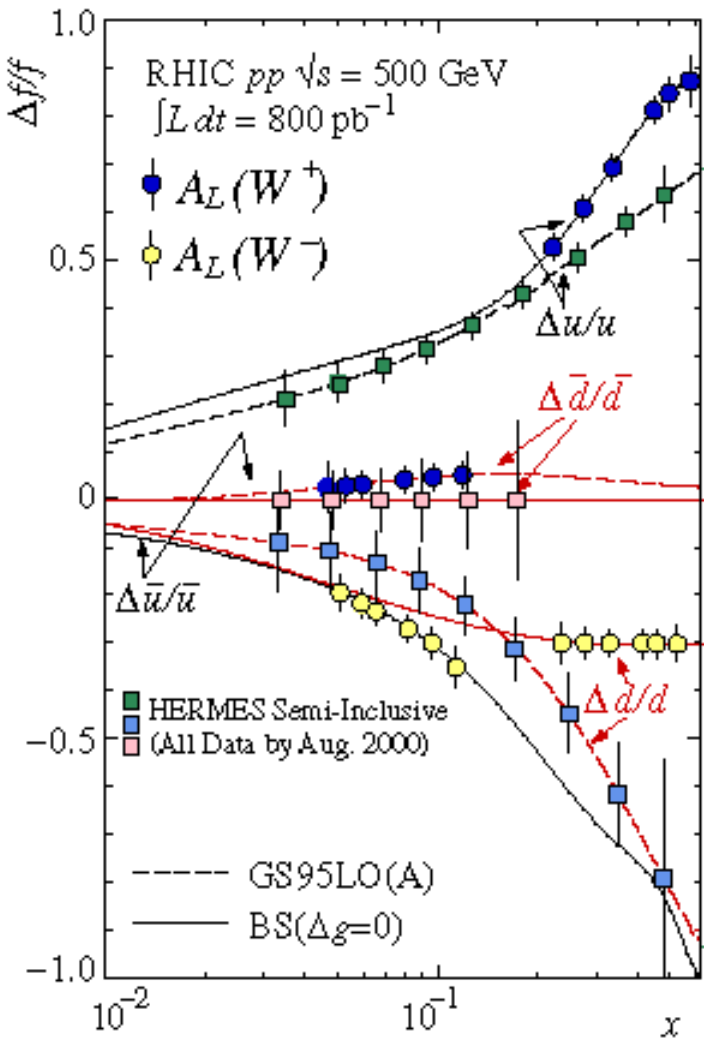

Figure 1.4.4 Expected statistical precision of spin-flavor decomposition using W boson single spin asymmetries.

Since the instantaneous rate of observed W decay leptons is not high, it is critical that the muon trigger have both high efficiency and discrimination. Specifically, it should be sensitive to the higher average momenta of the W decay muons and insensitive to muons resulting from hadron decay, especially from hard jets. Upgrades introducing muon fast tracking in level one trigger processors combined with nosecone calorimeter information to eliminate hadron jets off-line will provide the information necessary for carrying out the W physics program.

In addition to the studies of the spin-flavor composition of the nucleon, the addition of a nosecone calorimeter opens a new window on the measurement of ΔG through the detection of both the hadron jet and final state photon in the direct photon process. This would extend the capabilities of the PHENIX detector to allow the determination of the momentum fraction x_G of the gluon on an event-by-event basis, similar to that of STAR and more importantly, significantly extends the range of x_G given forward photon detection, roughly down to 0.001 at $\sqrt{s}$ of 200 GeV.

To date, this extraction has only been performed within a leading order (LO) QCD "framework", that is, with the effects of the Q^2 evolution only minimally included and no attempt at inclusion of higher twist effects. Several theoretical programs to extend the semi-inclusive analysis procedure to next-to-leading order (NLO) are underway. A chief concern with the HERMES analysis is the relatively low Q^2 (average about 2.5 GeV^2) of the data, which may result in large NLO corrections. The forthcoming analysis from COMPASS will certainly use a data sample with significantly higher Q^2 which will likely have smaller NLO corrections. Furthermore, it will extend the determination to almost an order of magnitude smaller x value than HERMES. Because COMPASS only will use a polarized deuterium target, some additional assumptions about the proton and neutron parton distributions will be required. Nonetheless, the HERA collider experiments have shown just how strongly coupled the resolution of the sea distributions are to the Q^2 of the probe, so it remains important to measure the spin-flavor composition of the nucleon up to the highest Q^2 possible.

References

[1] C. Bourrely and J. Soffer, Phys. Lett. B 314 (1993) 132.
[2] G. Bunce, N. Saito, J. Soffer, W. Vogelsang, Ann. Rev. Nucl. Part. Sci. 50 (2000) 525.
[3] P.M. Nadolsky and C.P. Yuan, Nucl. Phys. B 666 (2003) 31.

2 Design Considerations for the New Forward Detectors

2.1 Overview

In this section, we discuss design and R&D plans for the nosecone calorimeter (NCC) and two alternative upgrade options for the level one muon trigger. While the planning for the muon trigger and nosecone upgrades at the technical level can be carried out largely independently the integration of each subsystem with existing PHENIX detectors or future detector systems poses significant challenges. The NCC will occupy the space which is currently used for the nosecone hadron absorbers and will be located in the immediate neighborhood of the future fast time projection chamber (TPC) and the central and forward silicon detectors. The muon trigger upgrade is constraint by the existing muon spectrometer configuration including its wire chambers, hadron absorber walls and magnet yokes. For the muon trigger upgrade we discuss two options: first the modification of the muon tracker front end electronics in order to introduce information from the muon tracking stations into the level 1 trigger, second the construction of new dedicated level one trigger detectors. The discussion in this section gives a brief summary of our present thinking. The final design for the forward upgrade components will result from the ongoing R&D and simulation efforts and we plan that a detailed proposal will be available in January 2005.

2.2 Muon Trigger Upgrade

2.2.1 Motivation: Decay Muons and Beam Background

The PHENIX detector initially has been optimized for the needs of heavy ion physics. The collision rate for A-A running remains below 10 kHz, and the need for event selection arises only at higher trigger levels, resulting from data volume limitations in heavy ion collisions. However, for high-luminosity p-p and d-A collisions, it is essential to acquire additional low-level event selection capabilities. In particular, at full design luminosity, $L=10^{32}cm^{-2}s^{-1}$, for proton-proton collisions at $\sqrt{s}=500$ GeV the total cross section is 60 mb and the resulting reaction rate is ~12MHz. Therefore, powerful level 1 triggers with rejection powers of 5,000 to 10,000 are necessary in order to reduce the high raw collision rates in several rare event trigger channels to levels compatible with the available bandwidth (10 kHz) into the event builder.

At the high rates in proton-proton collisions, an upgrade of the muon level-1 trigger is required for nucleon structure studies utilizing W-production. The present level-1 muon trigger is based purely on muon identification. However, the trigger rate is dominated completely by muons resulting from hadron decays at low momenta, which leads to projected level-1 rates of about 30 kHz, well above the bandwidth limitations. Detailed simulation studies have shown that low-momentum decay-muons can be rejected by introducing muon momentum information into the level-1 trigger. We have studied two scenarios: I) the introduction of new dedicated trigger detectors located upstream and

downstream of the muon arm spectrometer magnet providing crude momentum resolution or II) instrumenting the existing muon tracker stations with new front end electronics which provides output to a local level one trigger processor. Both solutions have been found to provide sufficiently large rejection levels. A third possible solution appears to be a combination of a newly instrumented muon tracker station (I) and a new dedicated trigger detector downstream of the muon tracker magnet. At this time no decision has been taken in selecting a particular muon upgrade solution.

In addition to the collisions related muon background from hadron decays the trigger upgrade also has to solve the background problems which arise from beam losses and beam-gas interactions. During the 2003 d-Au and p-p 2003 runs beam related background levels were leading to peak single muon trigger rates above 20kHz. Significant efforts have been undertaken to improve the background situation: three four feet thick steel shielding walls were introduced in the beam tunnels up- and downstream of the PHENIX interaction region. Automated beam scraping procedures have reduced the background from beam losses. Background production resulting from vacuum contaminations caused by beam scrapping and beam gas interactions have been characterized and will be reduced through the introduction of neg-coated beam pipes. See section 3.3 of the PHENIX forward upgrade letter of intent for details on beam backgrounds.

Despite all efforts to reduce beam related backgrounds it still appears – based on the analysis of run 03 data - that a level 1 trigger based on muon identification, vertex pointing and momentum selection alone may be insufficient in order to discriminate beam related backgrounds from collision related muons. In particular early during RHIC fills background levels can be high prior to collimation. Assuming that beam related backgrounds in the muon spectrometers are dominated by background particles resulting from incoming beam scraping it will be possible to remove background with a timing cut. This represents a significant challenge with the present muon spectrometers as neither the muon identifier package nor the muon tracking chambers provide timing information. A new dedicated level 1 trigger detector with a timing resolution of a few nanoseconds would provide the required rejection. In this context we have considered scintillator hodoscopes as well as resistive plate chambers (RPCs).

2.2.2 Performance of the Present Muon Trigger

The rejection factor of the present MuID local level-1 trigger has been estimated using RUN3-pp data. The output information from the MuID ROCs are used as input to the package simulating the MuID deep symset algorithm which requires that a symset fires in both the horizontal and vertical direction. The results are shown as a function of run number in Fig. 2.2.1: The rejection factor of MuIDLL1 is around 250 and is significantly lower than the factor 1000 expected from the simulated – and therefore collisions related - data. The lower rejection of the trigger observed in the data is connected to beam related backgrounds. However, assuming that the shielding will be perfect and that we can reach the performance seen in simulated data, the rejection factor is still a factor of 10-50 less than that required to satisfy the upgrade requirement.

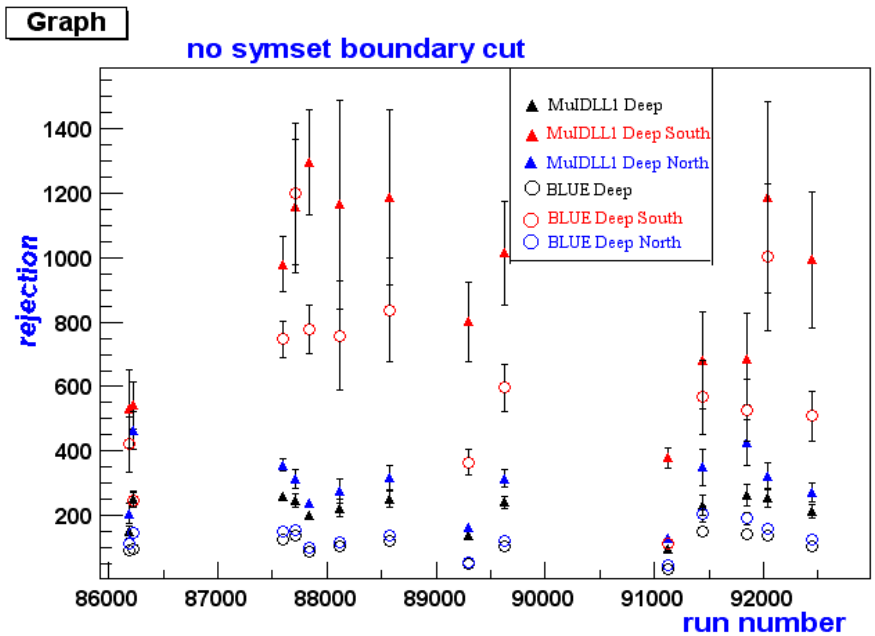

Fig.2.2.1 MuID LL1 rejection factor as a function of run number in RUN3-pp date. The triangles and circles represent the MuIDLL1 and Blue-logic trigger rejections, respectively. Red indicates rejection factors for the south arm and blue for the north arm. The black color shows the combined results of south and north.

2.2.3 Muon Trigger upgrade with RPCs

As explained in the previous section, the principle idea of the muon trigger upgrade is to introduce momentum resolution and timing information in addition to the muon identification provided by the present muon first level trigger. Muon identification is derived from the ability of muons to penetrate a sandwich of alternating Iarocci tube panels and steel walls which form the PHENIX muon identifier.

Off-line the muon momenta are determined from the track curvature through the muon spectrometer magnet based on hit information from the three muon tracker wire chambers located just upstream and inside the magnet. While muon tracker information is also available to the second level trigger the architecture of the front end electronics does not permit to send tracking information to the first level trigger processors. As a consequence the introduction of tracking information in the first level muon triggers will require either the re-design and re-building of the muon tracker front end electronics or the insertion of new dedicated trigger detectors. An additional complication in using muon tracker information comes from the difficulty to obtain sufficiently precise timing resolution for beam related background rejection. We assume that the timing resolution is limited by the intrinsic drift time to less than 30 ns.

Presently our simulation studies for dedicated new level 1 trigger detectors focus on a solution in which resistive plate chambers (RPCs) upstream of MuTr station I and downstream of the muon identifier provide the required tracking and timing resolution for

a momentum determination and beam background rejection in the first level trigger. RPCs have been introduced at RHIC successfully in a TOF application of the STAR experiment in run 2003. Led by the Vanderbilt group PHENIX has decided to utilizing RPCs for the planned expansion of the PHENIX time of flight detector. We are investigating the possibility to use identical or similar RPC technology for the muon trigger upgrade. This will require the development of new front end electronics including communication with a first level trigger processor. Additional comments on RPCs can be found in appendix C of the PHENIX forward upgrades letter of intent.

Each multi-gap RPC station carries two cathode planes; the first cathode has a coarse tile structure to establish a space point for correlation with the existing muon identifier, the second plane has radial cathode strips in order to provide the required azimuthal angular resolution. The two upstream stations (south and north muon arms) have external dimensions of about $1m^2$ and the total channel count is at 1620. The two downstream stations will be located in gap 5 for maximal protection from outgoing beam background. It is under study which area the downstream RPC stations needs to cover. Due to the smaller resolution required in the tile structure we expect a channel count lower than in the upstream station: 1120.

Hit and timing information from the RPC stations will be sent through optical fibers (standard PHENIX G-Link implementation) to first level trigger processors. The trigger processors will be based on the existing ISU local level 1 processor. Present applications of the processors exist in the muon identifier, the zero degree calorimeter and the EMC-RICH trigger in the central PHENIX spectrometer arms.

The proposed trigger detector configuration has been introduced in the PHENIX GEANT based detector Monte Carlo (PISA) and simulation results on expected trigger efficiencies and background rejection factors are available. We find that tile sizes of $10x10cm^2$ in the upstream RPC, $30x30cm^2$ and a angular resolutions of $\Delta\varphi=1^o$ lead to background rejections factors of 15000-20000 reducing the single muon trigger rates to about 0.5kHz well within the available bandwidth. See section 3.2 for details on the simulation.

2.2.4 Upgrade with a New MuTr-FEE

An alternative solution is to replace the muon tracker (muTr) front end electronics with new boards providing output information to a local level 1 trigger processor. The muon tracker is the only detector in the PHENIX muon system which is sensitive to the momentum of detected particles. The MuTr measures the deflection angle of the particle trajectory in the magnetic field running radially. The cathode strip runs also almost radially and measure the hit position in the azimuthal angle ϕ. Current readout electronics integrates the cathode signal for 4.0 μsec (40 beam crossings) to obtain a charge measurement with a reasonable resolution, which leads to the precision determination of the particle hit position to about100 μm.

We define *d* as the deviation of the hit in Station 3 from the linearly extrapolated point from the collision point and the hit in the Station 1. Figure 2.2.2 shows this deviation as

a function of momentum. In generating Figure 2.2.2, the vertex is distributed in Gaussian form with σ of 30 cm as observed in the real data and the signal is uniformly distributed in polar and azimuthal angle. A coarse selection of higher momentum particles can be performed by choosing small deviations *d*.

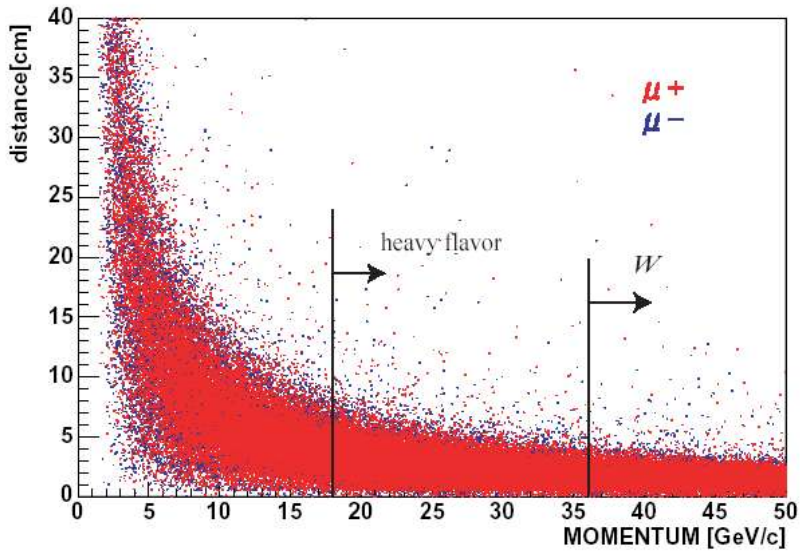

Figure 2.2.2 Distance or deviation of hits in the Station3 from the point extrapolated from the collision point and hits in the Station 1.

Technically this kind of trigger algorithm can be implemented as a lookup table of corresponding hits in Station 1 and 3. Since the algorithm assumes a fixed collision vertex, the table is static and thus simple. In Figure 2.2.3, the correlation of strip numbers in stations 1 and 3 is shown. The plot is made for muons with momenta of 15 GeV/*c*. The selection of higher momentum can be achieved by requiring a coincidence with the corresponding range of strip numbers in Station 3 for a given strip number in Station 1.

The performance of the proposed trigger using the Muon Tracking cathode signal has been evaluated using simulations as well as the real data from Run 3. The rejection factor is estimated to be ~2,700 to be compared to the required rejection of 5,000-10,000.

Further rejection can be obtained by measuring the sagitta by adding information from a third station to read. While fast tracking using only two stations was fragile against multiple scattering of lower momentum muons faking the high momentum muons, tracking with three points is found to be very efficient in excluding those fakes and will provide a rejection factor of ~20,000, which is already better than the required rejection factor.

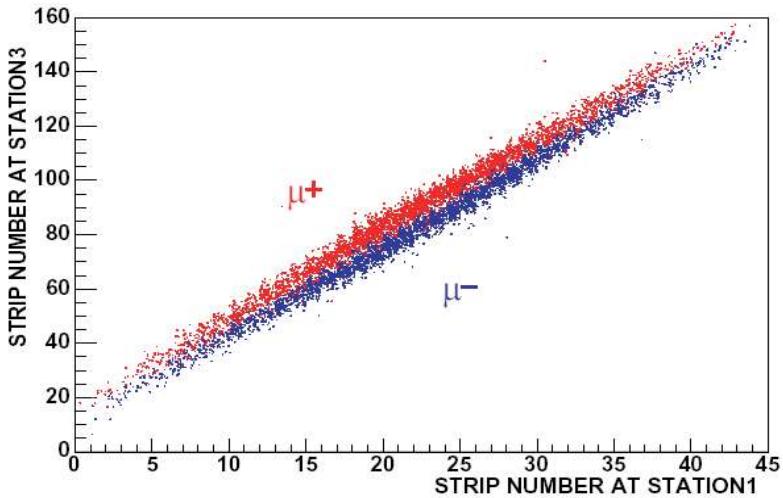

Figure 2.2.3 Strip numbers in Station 1 vs Station 3 for muons with 15 GeV/*c*.

2.2.5 R&D for a new MuTr FEE

To make use of the MuTr cathode pulses for level-1 trigger purposes, the pulse should be shaped into the 100-200 ns range, which is the beam crossing interval. This will be the major change of the front end electronics of the muon tracking chamber. Such a fast read out can be done either by adding new electronics in one plane out of six (four) planes in the 1st and 2nd (3rd) stations. On the other hand, we do not need to read out the cathode signal with high resolution for the level-1 trigger. We only need the center of gravity of the pulses with a precision of the strip pitch. This can be achieved by a readout with a coarse resolution (say 3 bits). Pulses usually are distributed between three or four strips. The geometric center of these strips is the closest strip to the actual hit position. Therefore it is very possible that using a one bit read-out, with a simple clustering algorithm would provide the required position resolution.

The Kyoto group had just built a test chamber with spare materials from the real PHENIX Muon Tracking Chamber (Station 1) at the University of New Mexico in close collaboration with the group at UNM. The chamber has been shipped to Kyoto University and the raw pulse shape for the fast read out has been studied. The first version of the new read out board has been ordered. The goal of this first version is to gain experience on the low noise read out and fast digitization, and to study possible problems with a high rate. In the second version, we would address the compatibility with the existing read-out board and PHENIX framework. We plan to have a first schematic design of the read-out board, in one year. Mass production could start around 2006.

2.2.6 RPC R&D

We have started a R&D project to study the performance of different RPCs at UIUC and RBRC. We have carried out measurements of collision- and beam-related backgrounds during the RHIC p-p run-4 and the analysis is underway.

As an immediate application for RPCs we consider using the detector technology for a new relative luminosity monitor for PHENIX (RLT). The RLT will replace the BBC as a relative luminosity monitor for very high luminosity p-p running. Resistive plate counters appear to be a possible choice since the proposed RLT requires good spatial resolution. The development of detector hardware and readout for the RLT RPCs will be identical to the hardware required for the muon trigger RPC and represents a convenient testing ground. We plan to test different types of RPC in the summer 2004 and build the RLT in 2005.

Collision- and beam-related backgrounds will be key factors negatively effecting the trigger performance. Understanding the nature of this backgrounds and it's magnitude is important input in finding the final trigger configuration among several possible choices. During the 2004 p-p run, we have measured background in both the central and forward rapidity regions with scintillators. The results will be compared to MARS beam background simulations and are expected to help in calibrating the simulation results. The shielding installed prior to run 04 has significantly reduced beam related backgrounds but remaining background levels still appear to be high. The background rates in different muID gaps has been measured during different running conditions and the MARS simulations show that most of the background seen by the muID results from slow neutrons which are absorbed by the PVC used in the muID Iarooci tubes.

In addition to the neutron background it will be important at higher luminosities to understand background contributions from beam related decay muons. The proposed muon trigger upgrade may have to include new dedicated trigger detectors with sufficient timing resolution to separate collision related products from incoming beam background as illustrated in Fig. 2.2.4.

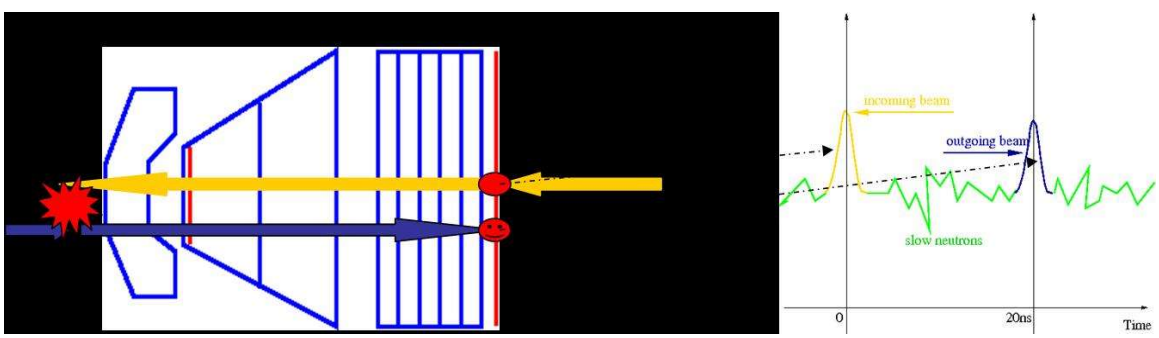

Fig. 2.2.4 Timing information can separate incoming beam background from collision related products. Outgoing beam background is in time with collision related products but attenuated by traversing the entire PHENIX detector.

However, collision products will occur at the same time as outgoing beam background. We hope to understand the time structure of the background from our 2004 background measurements. In particular it will be important to find out to what extend the material in the PHENIX detector attenuates the outgoing beam background.

2.2.7 Front End Electronics

New Front End Electronics (FEE) will be required to send hit and timing information for the new forward tracking detectors through optical fibers (standard PHENIX G-Link implementation) to first level trigger processors. A timing resolution of about 2ns will be required to reject beam related backgrounds. The two main upgrade options we are considering are to instrument the cathodes on the μTR stations or to build two new detectors upstream and downstream of the muon tracker magnets as described in the previous sections**:**

<u>New RPC detectors</u>

In this case we are considering building new electronics as the detectors will consist of a large number of channels (about 5000) and the time resolution requirement is modest ~2 ns. It has been roughly estimated to require one year of engineering time, with a total cost of $50 per channel for 5000 channels. It is relatively inexpensive as the timing at these resolutions can be achieved using buffering rather than TDCs.

<u>Instrument μTR cathodes</u>

The current architecture of the μTR front end electronics does not permit to send tracking information to the first level trigger processors. As a consequence the introduction of tracking information in the first level muon triggers will require the redesign and rebuilding of the μTR FEE. The necessary R&D is being carried out at Kyoto University, see section 2.2.5. .

2.3 Nosecone Calorimeter (NCC)

2.3.1 Conceptual Design

As demonstrated in the preceding chapters of this proposal the physics places considerable demands on the detector which must be capable of measuring photons and jets, providing hadron – electron separation, and aid in the tracking of muons from J/ψ and heavy flavored particle decays close to the collision vertex in high multiplicity events. Reaching all these goals within the envelop of the existing PHENIX magnet nose cones is a challenging task. This chapter describes a reasonable compromise which will allow us to start a physics program on a relatively short time scale and to expand it at

later stages when all components of a planned detector system will actually become available. It calls for a new calorimeter which replaces the current nosecones on the two muon arms. Conceptually each nosecone consists of 3 elements

a) an electromagnetic calorimeter in the front
b) a shower max detector
c) a crude hadronic calorimeter

A single technology is chosen for all three sections for ease of construction.

2.3.2 Detector Layout and Configuration

The location of the proposed Nose-Cone calorimeter together with the new central tracking detectors is shown in Figure 2.3.1.

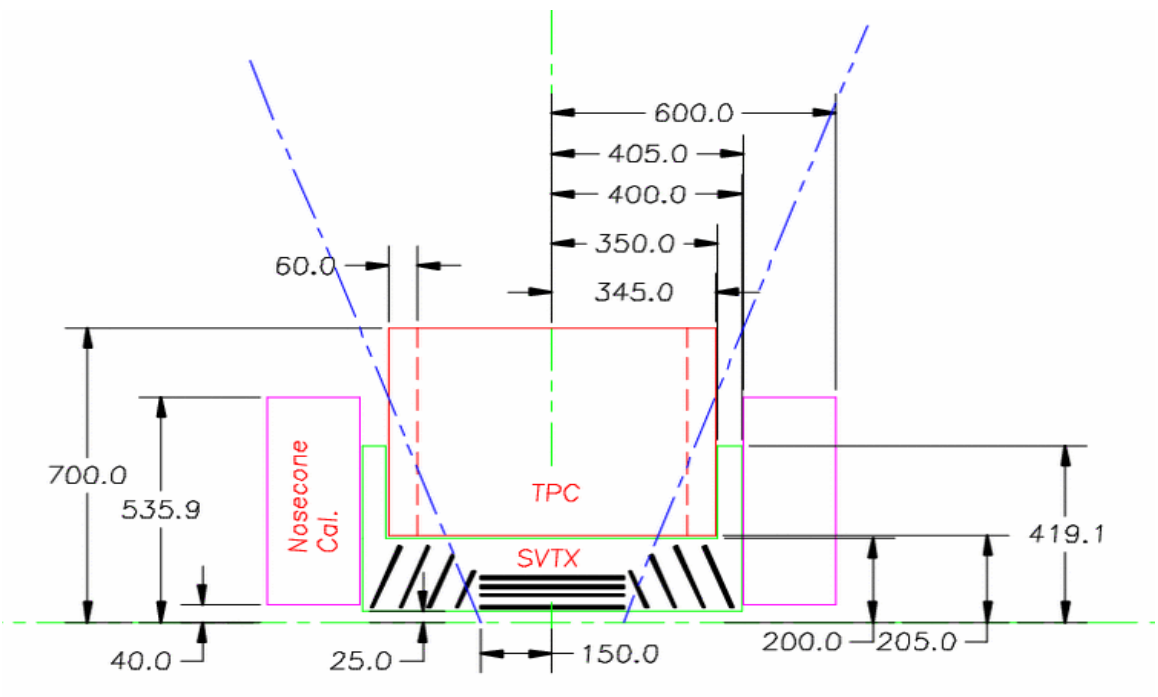

Fig. 2.3.1 Sharing of the space budget between new detectors in the central PHENIX region.

Available real estate is shared between the forward silicon tracking, the central silicon vertexing system and the tracking TPC. The NCC will occupy the space along the collision axis which is currently used to install supplementary muon filters (NoseCones, one for each magnet pole) consisting of Cu disks 19 cm deep and ~ 1m in diameter. The depth of the new calorimeter is chosen to fit within the envolope of the existing Nose Cones. We propose to build two identical devices for the North and South Arms of PHENIX.

As a component of the PHENIX Forward Spectrometer the NCC is expected to provide for or contribute to the following:

1) precision measurements of individual electromagnetic showers;
2) photon to π^0 discrimination similar to the central PHENIX electromagnetic calorimeters;
3) photon/hadron discrimination;
4) jet finding and jet energy and impact position measurements;
5) data for fast triggering.

This will require a combination of a highly segmented electromagnetic and hadronic calorimeters supplemented by high resolution position detectors located (a) upstream of the calorimeter and (b) at the depth in the calorimeter corresponding to 100% probability for both photons from π^0 decay converted and seen in the detector.

We propose to build the NCC as a super dense sampling calorimeter using an absorber with the shortest possible Moliere radius which is a W/Cu alloy called "heavymet". At least a few % of Cu is required to allow for easy machining of the complicated shapes out of otherwise very hard W sintered ingots. The choice of a W results in a very short radiation length and a large absorption/radiation length ratio limiting electromagnetic shower development to the very first few cm of absorber. This allows us to implement both the electromagnetic and shallow hadronic compartment within the available space. A shower max detector (SMD) is located in one of the gaps of the calorimeter to aid in the separation of close photon showers from π^0 and to add an additional point for tracking muons. Table 2.3.1 summarizes the goals of our design. Table 2.3.2 shows the implementation of these goals.

Observable	**Featured parameter**	**Goal**
Photons	EM resolution	~20%
	position resolution	~3 mm to be comparable to central calorimeters
	Hadron rejection	better then 100
Electrons	Upstream tracking	impact position known to better then 1 mm
Muons	Upstream tracking and /or tracking inside NCC	few points on muon trajectory measured with sub mm resolution
Jets	Depth	~2 $\lambda_{Absorbtion}$
	Acceptance	$0.9 < \eta < 2.5$
	Multiple shower separation	few cm

Table 2.3.1 General considerations important to designing the Nose Cone Calorimeter System.

Parameter	Value	Comment
Beginning Z-coordinate	40 cm	
Radial coverage	50 cm	
Geometrical depth	~20 cm	
Absorber	W	(16 x 2.5 mm + 6 x 16 mm)
Readout	Si pads	Single readout layer is 2.5 mm thick
Sampling cells	22	EMC(16 x 0.5cm) + HAD(6 x 1.85 cm)
Longitudinal segments in readout	3	Summation over 6 – 10 – 6 sampling cells
EM compartment (Rad length)	9	
Total depth (Rad length)	~40	
Total depth (Abs length)	>1.5	
Multiple scattering (MeV) in NCC combined with Fe magnet pole	133	Compared to 106 MeV in the existing configuration with Cu NoseCone
Expected EM energy resolution	20%	
Tower size (cm)	1.5 x 1.5	Nonprojective
Two showers resolved at	3cm	
Shower max detector (SMD)	In gap 6	Two orthogonal layers of silicon strips
Shower max granularity (mm^2)	2 x 60	
Two showers resolved at	0.3 cm	

Table 2.3.2 Parameters of the W/Si Nose Cone Calorimeter

2 longitudinal sampling cells (layers) each of tungsten and silicon are held together by the tightening rods threaded into the central magnet poles. The tungsten in the first 16 cells has a thickness of 2.5 mm (~0.7 X0), and 1.6 cm in the remaining 6 layers serving as a crude hadron calorimeter. The interleaved readout layers are 2.5 mm thickness comprised of 0.3 mm silicon, 0.8 mm of G10 (motherboard), 1 mm space is reserved for preamplifier chips (no packaging) and a 0.2 mm air gap which will probably be mostly used by protective mylar sheets on both sides of readout unit. The readout gap after layer 6 has a triple thickness to accommodate two layers of SMD silicon strips. We are planning to use the same size sensors both in the calorimeter and in the SMD. The surface area of an individual strip is currently chosen to be half of that for the pad (~120 mm^2). The need for an SMD is dictated by the fact that the calorimeter starts at a distance of only 40 cm from the collision point and will be unable to separate two photons from π^0 decay for any momenta above ~2 GeV/c. The SMD will raise this limit to 10-15 GeV/c depending on the vertex position and decay configuration, and will provide additional rejection power for /hadrons. It will also serve an important tool for jet energy measurements, providing extra constraints on the longitudinal localization of hadronic showers. It will also complement the forward tracking allowing a better match between tracks in the forward silicon and in the muon tracking system.

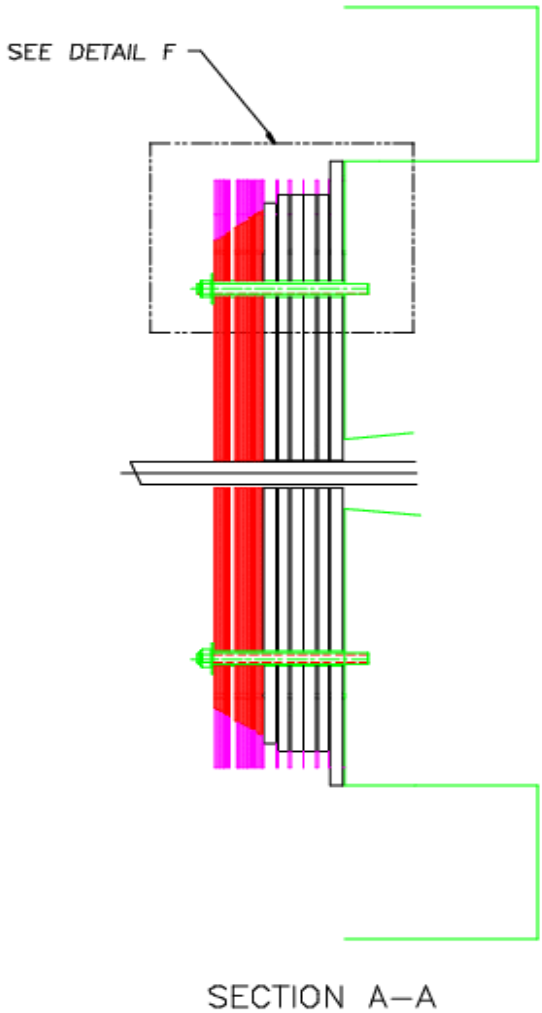

Fig 2.3.2 Conceptual design of the PHENIX Nose Cone Calorimeters.

Simulation work is still required to optimize the NCC structure for the following tasks:

(1) measuring electromagnetic showers with a reasonable resolution;
(2) measuring shower cores at a shower max depth to separate single photons from photon pairs due to π^0 decays;
(3) early containment of the electromagnetic showers and shower shape measurements to do electron/photon identification;
(4) measuring energy leakage from electromagnetic compartment allows for greatly improved rejection of hadronic showers;
(5) jet finding, precision measurements of the jet direction and rough estimates for the total jet energy;
(6) separation of the jet energy depositions due to photons from those due to charged particles;
(7) serving to improve background conditions in the muon spectrometers;
(8) serving to improve J/psi effective mass resolution.

The mechanical design and layout of the sensors and readout units was optimized to minimize the number of different sensor geometries and readout unit configurations. A careful consideration of different mechanical layout schemes ended in selecting the most trivial one: identical width horizontal pockets formed by tungsten layers and 2.5 mm thick narrow spacers. Each pocket is occupied by identically structured readout units carrying at most 16 (2x8) sensors, either square or with one corner designed to accommodate load-bearing bolts and the RHIC vacuum pipe penetrating the whole depth of the calorimeter (Fig. 2.3.3).

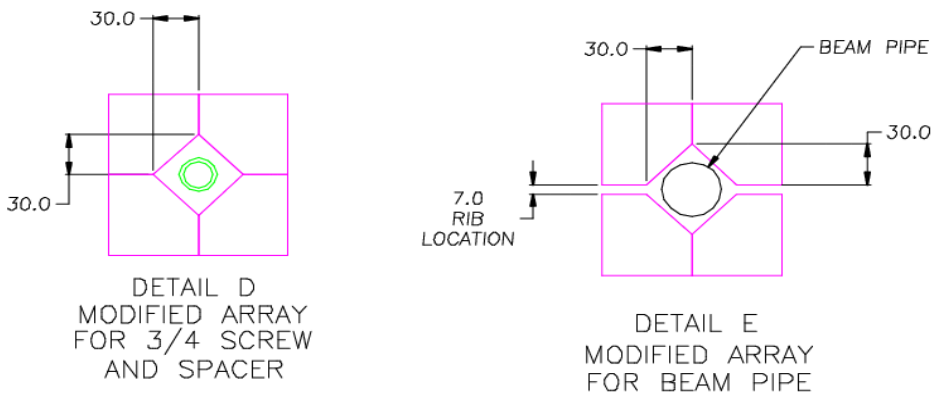

Fig. 2.3.3 Silicon sensors with chamfered corner used in the areas of tightening rods and around beam pipe.

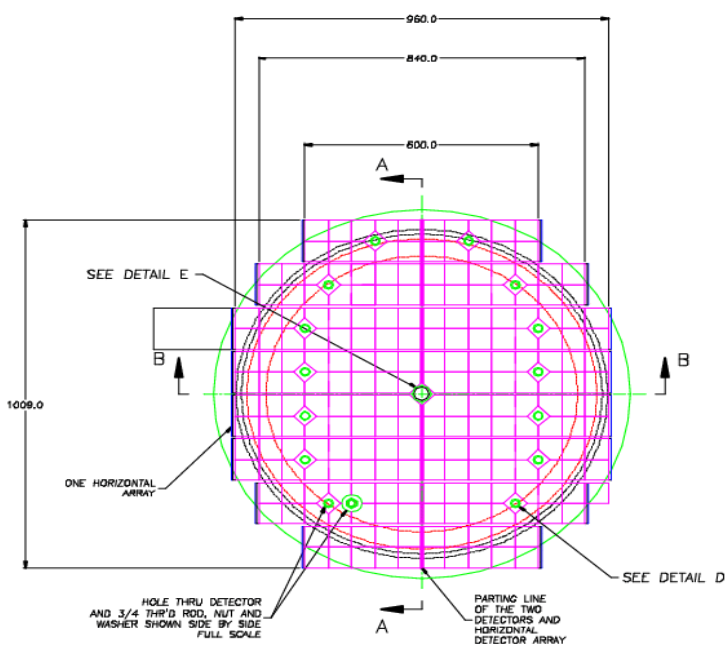

Fig. 2.3.4 Geometrical layout of sensors in readout layers of the NoseCone Calorimeter.

The detector will require 3 kinds of readout units. All are two sensors wide but different in the number of sensors are installed along the long side. The layout of all readout units are identical and shorter units will have a number of readout lines unused.

The squares in Figure 2.3.4 are silicon sensors with the silicon area divided into 16 squared p-n junctions AC coupled to the front end electronics. The next table explains in greater detail some of the choices made with regards to the dimensions and numbers of sensors and pixels in the proposed detector.

Parameter	**Value**	**Comment**
Sensor size (cm)	6 x 6	to maximize the yield
Pixel size (cm)	1.5 x 1.5	to match molier radius and to reduce channel capacitance
Pixels per sensor	16	
Maximum number of active sensors in the sampling layer	216	
Sensors in the detector	3656	
Total area of Silicon (m^2)	13	
P/A granularity	32 channels	
Chips / sensor	0.5	
P/A channels / layer	<3500	
Readout channels	~10000	
Dynamic range (MIP's)	100 to 500	The 500 dynamic range is to cover the range of species available to PHENIX

Table 2.3.3 Silicon detectors for the electromagnetic and hadronic compartments of the W/Si Nose Cone Calorimeter.

Developing and prototyping readout units carrying these sensors will be the main subject of the R&D program proposed for the first calendar year of this project. Some of the important parameters of the readout units are listed in the Table below (Table 2.3.4).

Parameter	Value	Comment
Sensor Dimensions	12 x 55 cm2	
Sensors, max	2 x 8	
Signal lines at the readout unit edge	256	
Line spacing	0.17 mm	

Table 2.3.4. Specifications for the readout unit.

To make use of shower compactness in W the calorimeter needs to be appropriately segmented both laterally and longitudinally. Segmenting the detector longitudinally at a maximum shower depth and at the start of the coarse compartment as proposed in Table 2.3.1 provides a reasonable compromise between needs of physics and readout cost .

2.3.3 Event Environment in NCCs

Since the NCC is close to the production vertex, the calorimeter will need to work in at high occupancy, especially in central Au-Au collisions. The current proposal for the lateral granularity of the calorimeter is based upon simple analytical computations of the probability for a sensor (or strip in the shower max detector) to be fired by the shower. The calculations were made assuming the worst possible scenario: it was assumed any shower in the calorimeter would fire a base matrix of 3x3 towers and 3 neighboring strips in the SMD. The strips and towers were assumed to be of a similar surface area (~200 mm^2). The resulting radial (from the beam) dependence of the probability for strips in the SMD and towers in the calorimeter to see event related energy is plotted in Figure 2.3.5 below.

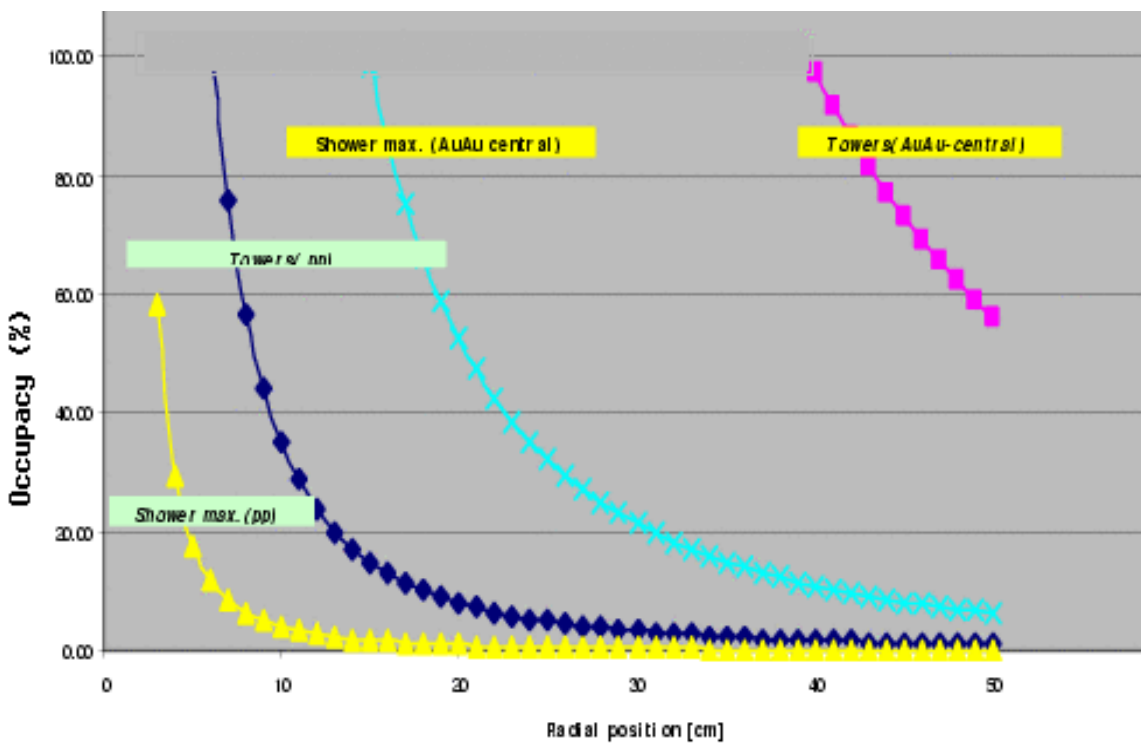

Fig. 2.3.5 Probability for tower in NCC and strip in SMD to be fired (occupancy) in AuAu collisions in PHENIX as function of the distance from the beam pipe.

In pp collisions, conditions similar to those in the central calorimeter are reached at a radial distance of 10 cm hence the entire calorimeter area will have a reasonable occupancy. The beam pipe assumed to be 4 cm in diameter. Running conditions are certainly less favorable in AuAu collisions where the calorimeter will be heavily occupied by the showers due to soft secondary particles. The SMD occupancy still stays relatively low allowing for cluster counting and impact point measurements in the calorimeter allowing jet finding based upon hit occupancy even in the events of highest multiplicity.

Energy measurements in AuAu collisions will be strongly affected by the pileup from underlying events resulting in higher threshold values and additional inefficiencies. Simillar problems are seen in the present central caloimeters. In this respect the most challenging part of the NCC program is jet measurements. Multiple approaches such as threshold selected hit counting, energy profiling and energy flow which requires tracking the momenta of charged particles will be used. The next figure (Fig. 2.3.6) is a crude example of what to expect in pp collisions.

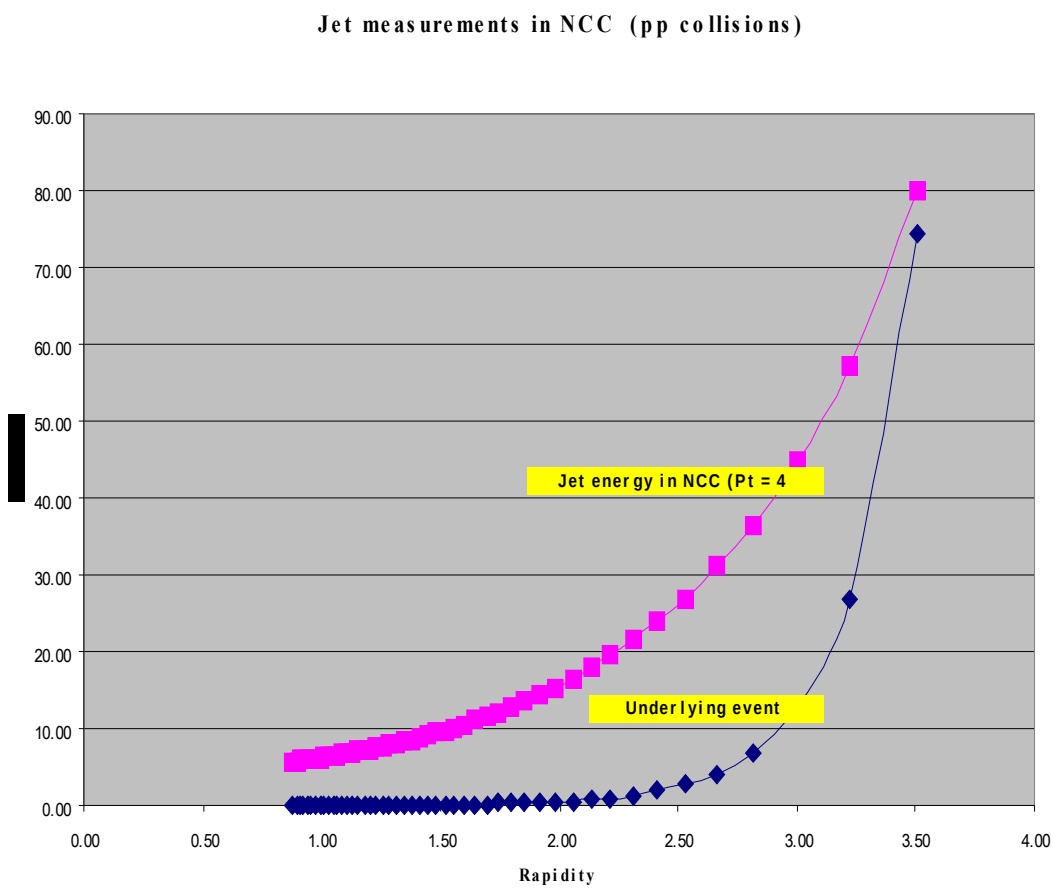

Fig. 2.3.6 Effect of the underlying event on the jet measurements in the Nose Cone Calorimeter in pp collisions at RHIC.

Depending on the rapidity, a 4 GeV/c transverse momentum jet in the NCC acceptance window will have a total energy of 8 GeV to 80 GeV. It will be seen in the calorimeter with very little pileup contribution up to ~2.5 units of rapidity and will start merging with the underlying event only at rapidity ~3. In pp collisions a dense relatively shallow calorimeter will see high pt jets as easily identifiable, narrow peaks in the energy profile.

Due to the background from underlying events in Au-Au collisions, there will be more smearing to the energy profile which will move the threshold for identifiable jets to somewhat higher transverse momenta.

2.3.4 Effect of NCC on Muon Measurements

It is important that we understand and minimize the impact of the new calorimeter on mass resolution of the current muon arms, since the J/ψ is one of the most important components of the PHENIX physics program. Indeed, one of the goals of the NCC is to allow the measurement of the χ_C which decays to a J/ψ and a photon. As mentioned previously, the resolution of this state is primarily dictated by the resolution of the J/ψ . Hence special efforts were made to study the potential impact of replacing existing brass Nose Cones with a calorimetrized detector of a much larger depth (measured in units of radiation length). The effect of this change can easily be understood from the next Table which compares a few basic numbers for NCC and existing Nose Cones.

	Cu Nose Cone	NCC
X0(total)	13.3	39.2
λ_{abs}(total)	1.26	1.5
dE/dx(total)	195 MeV	390 MeV
J/ψ width (GEANT)	155 MeV	178 MeV
Mult. Scattering (Cu+Fe pole, GEANT)	100 MeV	
Mult. Sc. (Cu+Fe pole, estimate)	106 MeV	133 MeV
Struggling & measurements	118 MeV	~118 MeV

Table 2.3.5 Comparison between scattering impacts on J/ψ resolution due to existing Cu Nose Cones and NCC.

GEANT was used to get an estimated J/ψ resolution in PHENIX in the absence off multiple scattering (due to Landau fluctuations and measurement errors) equal to 118 MeV. The contribution due to multiple scattering then can be estimated by subtracting this value quadratically from the J/ψ total width and is equal to 100 MeV. A trivial estimate based upon the number of radiation lengths of material in 19 cm Cu and 60 cm Fe (magnet pole) gives 106 MeV for the same value. The corresponding estimate for the NCC calorimeter is 133 MeV leaving the straggling contribution almost unaffected. The same GEANT simulation has shown a 5% loss in the number of reconstructed J/ψs consistent with expectations due to 200 MeV increase in the momentum cutoff due to ionization losses. More details on the simulation can be found in the appendix of the PHENIX forward upgrade letter of intent.

As one can see from this table, replacing the existing Cu Nose Cone with the calorimeter will add 23 MeV to the J/ψ width, if we presume that no effort is made to use the SMD and/or forward silicon to improve J/ψ mass resolution. The absence of this tracking today is exactly the reason why multiple scattering contributes so heavily to the J/ψ width. While straggling contributes to muon momentum uncertainties, multiple scattering is responsible for angular (or muon transverse momentum) measurement uncertainties. If muon trajectories upstream and downstream of the major scatterer (Fe magnet pole) are

matched and the muon directional vectors measured upstream are used to compute the J/ψ effective mass, the multiple scattering contribution can basically be eliminated. This approach will certainly work in pp collisions. Testing its efficiency in AuAu central events will require further simulation. Additional discussion can be found in section 3.1.

2.3.5 FEE (Readout, Signal Packaging and Processing)

For readout purposes the calorimeter is longitudinally segmented into two fine and one coarse sections (two electromagnetic and one shallow hadronic compartments). Since we are very far from the final detector design, the current readout concept should be considered very fluid, mostly educated guesses based upon what is known about similar implementations for calorimeter-type detectors elsewhere. The silicon tungsten calorimeter described in the above section will have close to 80 000 silicon pixels. This calls for a compact, economical readout. To control cost and complexity, we seek an integrated solution, where one channel of electronics serves a large number of pixels and the electronics is compatible with the NCC mechanical structure and the real estate sharing between different components of the PHENIX central detector upgrade project. Given a relatively modest requirement on energy resolution in the NCC's we consider digitization of signals from individual pixels unnecessary and opt for passive summation of the amplified currents due to shower signals in sequential detector layers.

Fig. 2.3.7 illustrates two different approaches to the initial stage of signal processing (amplification) we currently consider: DC (all current is handled in the input amplifier) and AC (using bypass capacitor) coupled detector pixels. The DC coupled diodes could be used only if we are certain that the current limit set by the readout chip design (reasonable assumption of 100 nA per channel) is never reached.

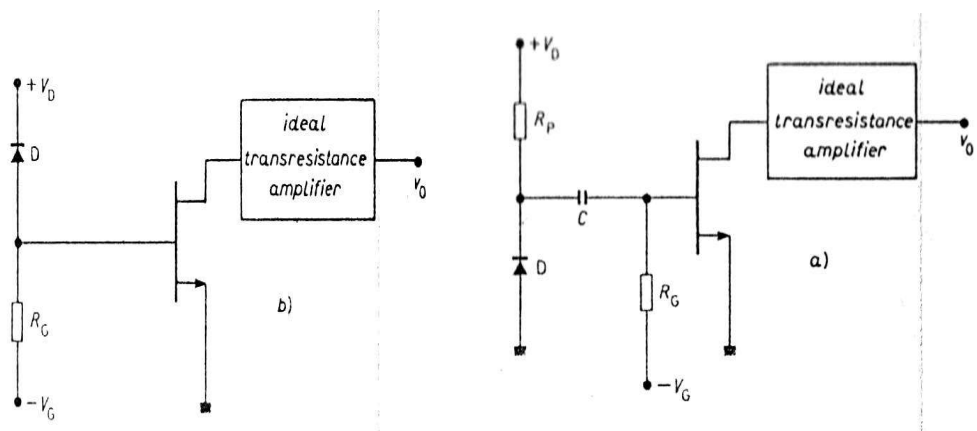

Fig. 2.3.7 Two approaches to signal processing are shown.

The AC coupled devices are in many aspects safer for the preamplifiers but require bypass capacitances at least x10 higher then intrinsic capacitance of the diode.
While waiting for the conclusions from our recent exposure of silicon diodes to the PHENIX radiation environment in the space between the existing Nose Cone and beam

pipe, we will consider for the purposes of this LOI the case of the total fluence of 100 kRad(Si) or about $3*10^{12}$ equivalent neutrons per cm^2. For a pad size of the order of a few cm2 and 300 mkm sensor thickness, published data (Fig.2.3.8) predicts the leakage current of the order of 5 – 10 mkA per pad or at least an order of magnitude higher then the limit set at the beginning of this chapter.

To avoid the potential of failure we are proposing to use AC coupled sensors in the NCC. This decision is unusual for pad sensors, since all large area sensors currently used in calorimetry are DC coupled devices connected to preamplifiers via blocking capacitors. Extreme space constraints of the PHENIX geometry force us to opt for an integrated solution , which is the only available approach to avoid mounting 16 high voltage (relatively big size) capacitors per sensor on every readout unit.

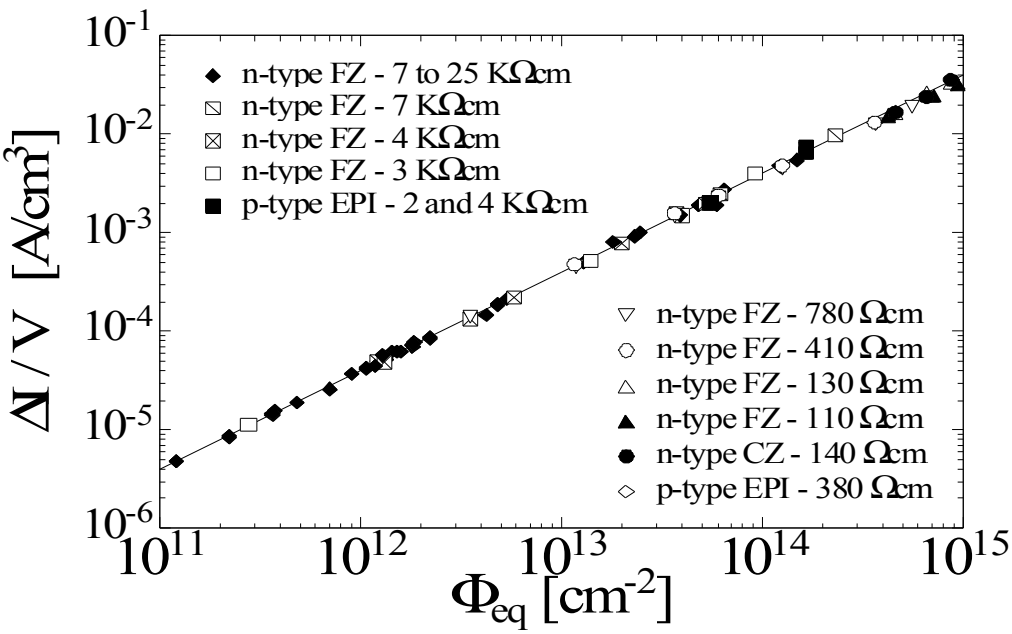

Fig. 2.3.8 Increase of leakage current with fluence for different types of materials.

We will sum up 6, 10 and 6 depth-sequenced pixels in the first, second and third longitudinal sections of the calorimeter. We will use custom flexible cables with a layout similar to the readout unit motherboard layout. It is typical for similar applications to have one end of this cable to serve as an extension to the outer edge of the readout units. Another end of the cable will be plugged into the zero insertion force connector on the adaptor/sumer board positioned in close proximity to the detector (Fig. 2.3.9). Given the density of the lines on the edge of readout unit we are not planning for any connectors on the readout unit itself . Rather modest goals for the electromagnetic energy resolution as set in this proposal allow us to disregard the potential contribution to resolution due to the spread in the gains between individual channels and or preamplifier chips. Summing up the amplified currents allows us to control the capacitive noise due to the increased detector capacitance.

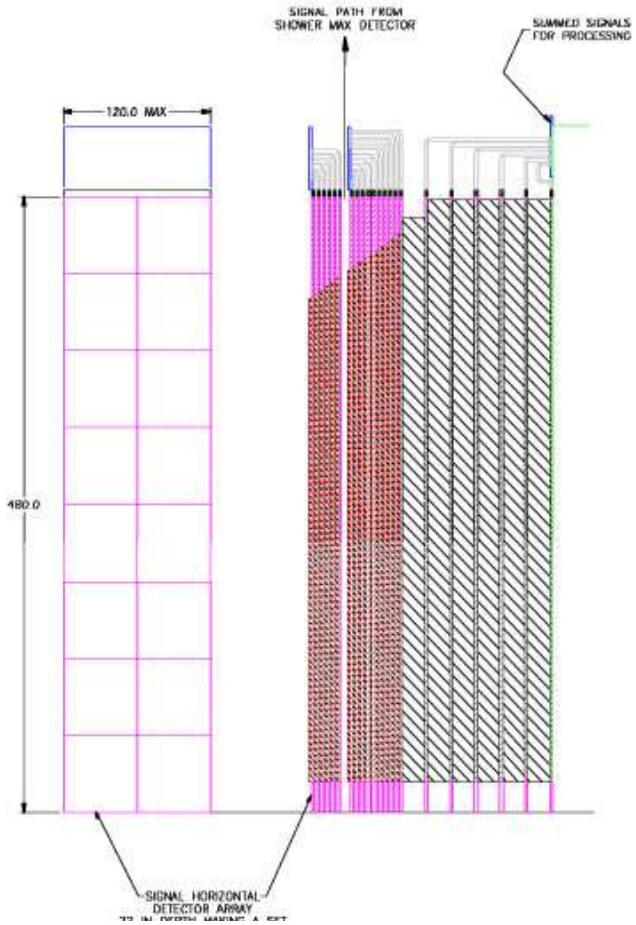

Fig. 2.3.9 Possible arrangement for the passive summing adaptor boards collecting signals from individual NCC pixels.

Each readout unit will deliver 256 signal lines to an adapter board. The number of lines actually in use will depend on the unit location in the detector and can be as low as 160 for the top and bottom rows. Following the declared intent to minimize the number of individually designed components in the detector, we are planning to use the same design everywhere for the adapter boards, 352 boards in total, each sending 256 summed outputs to signal processing and trigger logic electronics.

2.4 Local Level-1 Trigger Electronics

In order to pursue it's rare-event physics program the PHENIX experiment requires high luminosity from the RHIC accelerator and highly selective Level-1 and Level-2 trigger systems. In particular, the Level-1 trigger system is limited to a maximum rate of 12.5kHz by the readout rate of the detector front-end electronics. This will require an overall event rejection of up to ~1000 when RHIC reaches its goal of ten times design luminosity for protons in future runs. Since we anticipate the parallel acquisition of several rare event channels, the rejection for an individual trigger channel must be larger by a factor 5-10. The PHENIX Level-1 trigger is fully pipelined and provides an event

decision in less than 4.2μs (40 RHIC clock ticks).

The PHENIX Level-1 Trigger is a parallel, pipelined trigger system designed to provide a highly configurable trigger capable of meeting the demands of the PHENIX physics program. The Level-1 Trigger consists of two separate subsystems. The Local Level-1 (LL1) systems communicate directly with the participating detector systems. The input data from these detector systems is processed by the LL1 algorithms to produce a set of reduced-bit input primitive data for each RHIC beam crossing. The Global Level-1 system receives and combines this data to provide a trigger decision. In addition, busy signals (both global and trigger) are managed by GL1. The PHENIX detector system readout is divided into two sets of elements: *granules* and *partitions*. A granule is the smallest detector element that communicates with the PHENIX timing and control system via a Granule Timing Module (GTM). The GTMs distribute the local 9.4Mhz RHIC beam clock as well as control bits and event accepts to the granule. A partition is an administrative configuration of granules that share both busy signals and Level-1 triggers.

In this PHENIX upgrade the nosecone calorimeter (NCC) LL1 primitive system will generate primitive information on the jet axis, as well as single and multiple high energy clusters. A possible muon tracker LL1 system will generate primitive information on the momentum of high p_T tracks.

The MuID LL1 system is based on a generic, configurable LL1 trigger board designed and built by Iowa State University. The Generic Local Level-1 hardware (GenLL1) was designed to address a number of difficulties faced in extending the original design concepts for LL1 systems to address the full range of PHENIX trigger needs. First, the hardware had to be re-programmable to allow not only quick corrections to the trigger logic, but modifications of the trigger system as the PHENIX physics program evolved. This also had the added advantage of lowering development costs and allowing quicker prototyping of new trigger systems. Second, the new hardware had to be able to manage a data throughput of ~20Gb/s in order to be able to handle large data volume detectors (such as the Muon Identifier) without prohibitive cross-stitching between multiple boards (and crates of boards). Finally, in order to keep power consumption and heat load on the board within reasonable limits the GenLL1 design was required to use the next generation of HP GLINK receiver/transmitter logic (the HDMP 1032/1034), which runs at 3.3V. Smaller format transceivers (Agilent HFBR 5912) were also required in order to be able to handle up to twenty fiber inputs on a single 9U VME board. A complete description of the GenLL1 hardware can be found elsewhere.

In order to maximize the trigger rejection at Level-1 it will be necessary to combine trigger information from all of the forward Level-1 systems. In order to accomplish this, a new regional trigger processor will then take the complex trigger primitive information from the nosecone calorimeters, muon tracker systems and muon identifiers, combine the individual detector LL1 primitives, make trigger decisions and send them to GL-1. A block diagram of the data flow is shown in Figure 1. In order to pass data between the regional trigger processor and the LL1 systems efficiently it may be possible locate all the Level-1 trigger systems in a single crate and make use of a high-speed 16-bit data bus that is already available in the GenLL1 design to transfer the trigger primitives.

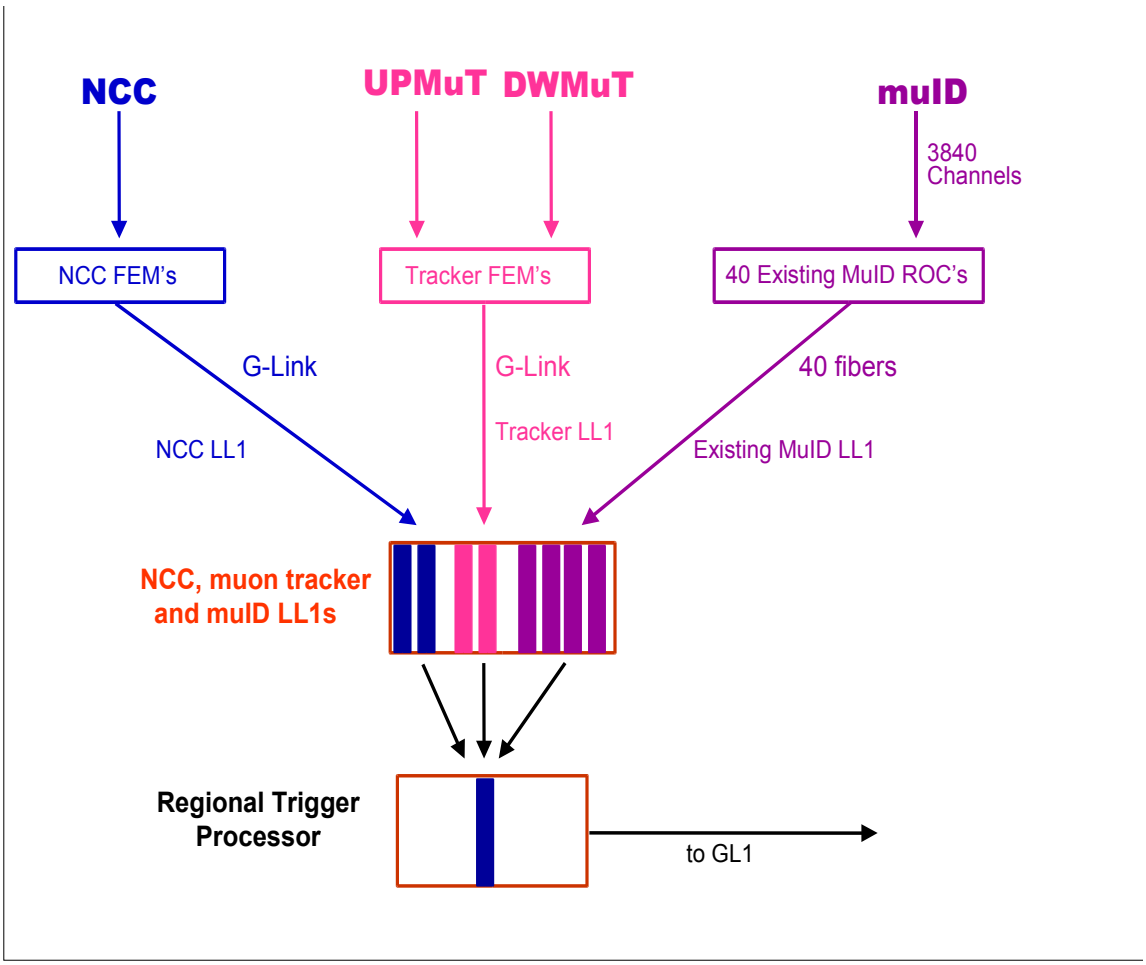

Fig. 2.4.1 Block diagram of the combined forward PHENIX Level-1 trigger system showing the nosecone calorimeter, NCC, trigger muon tracker stations and the existing MuID LL1 system for a single PHENIX muon arm. In order to combine the primitives of the various trigger systems a regional trigger processor will combine the trigger information before sending primitives to Global Level-1.

2.4.1 The NCC Level-1 Trigger System

The nosecone calorimeter (NCC) will use a Local Level-1 (LL1) trigger to select events via with a high p_T photon or jet in the calorimeter acceptance. As is typical of PHENIX LL1 systems the processing will consist of a set of pipelined stages. First, a set of primitive data will be digitized on the front-end modules (FEMs). Second, this data will be transferred to an LL1 system, and finally the bit-reduced trigger information is sent from the LL1 system to the PHENIX Global Level-1 trigger system; possibly via a new regional trigger processor to combine level 1 information from the different forward detector systems.

The NCC system consists of over 10k channels of analog data per nosecone spread over three layers in depth. The FEMs will combine calorimeter towers into non-overlapping 2x2 trigger tiles, digitize the output, and pass the LL1 system an 8-bit ADC value per trigger tile. The 8 bits per channel will allow a ~400 MeV least count with a full range of 100 GeV, and will result in an aggregate bandwidth of 200Gbit/s per nosecone into the LL1 system, roughly a factor of 5x larger than the data processing capacity of the existing MuID LL1 system.

Because of the large data volume and tight space constraints on the detector FEMs we are considering the possibility of transferring the data over high-speed serial links into an LL1 system located in the detector hall, as opposed to other LL1 systems that transmit their data over optical fiber links to LL1 electronics in the PHENIX rack room. The advantage of this approach would be that with serial links we could concentrate the entire NCC LL1 data stream into a smaller number of LL1 modules, simplifying the data cross-stitching required for jet cluster trigger algorithms. This would only be possible by using high-speed copper serial links between the detector FEMs and the LL1 electronics which are inherently short-range, requiring the LL1 electronics to be located in the detector hall.

The LL1 system would process the NCC 2x2 data to provide a set of photon triggers and jet cluster triggers based on the 2x2 trigger tiles, where both sets of algorithms would operate both laterally and using the depth information in the NCC to provide clean photon triggers. Detailed simulations of the performance of the NCC LL1 system are underway. The reduced bit output of the NCC LL1 trigger, in the form of a set of bits indicating satisfied algorithms, would be transmitted to the GL1 system over optical fiber.

3. Collaboration

Since the forward upgrade project encompasses both heavy-ion and spin physics interests, the group of collaborators includes people from both the heavy-ion and medium-energy communities in PHENIX. Table 3.1 below lists the institutions presently collaborating and their stated interests.

Beyond the present participation, we are engaged in discussions with a variety of European institutions in particular, INFN Trieste (Andrea Vacchi) and INFN Frascati (Pasquale DeNizza). Both of these institutions may bring a significant number of collaborators. There is also the possibility of securing international funding connected with these groups. We also attempt recruiting from experimental groups at DESY and possibly at CERN since the deep-inelastic experiments Hermes, H1 and Zeus will be completed in the near future. We are aware of several groups in HERMES and COMMPASS with specific interest in RHIC spin projects. However, at the present time the uncertainty in the GSI schedule and funding scheme make it difficult for most European intermediate energy groups to gain significant funding commitments for RHIC related projects at the present time.

US Institutions	**Interest**	**People**
Brookhaven National Laboratory	Nosecone Calorimeter	Edward Kistenev
University of California, Riverside	Muon-Trigger+ Nosecone Calorimeter	Ken Barish, Richard Seto, Stefan Bathe, Xinhua Li, Astrid Morreale Alexander Solin
University of Colorado	Nosecone Calorimeter	Ed Kinney, Jamie Nagle, Frank Ellinghaus
Nevis (Columbia)	Front End Electronics	Cheng Yi Chi
University of Illinois Urbana Champaign	Muon-Trigger+ Nosecone Calorimeter	Alex Linden Levy, Cody McCain, Jen-Chieh Peng, Mickey Chiu, Ralf Seidel, Joshua Rubin, Matthias Grosse Perdekamp
Iowa State University	Level 1 Electronics	John Hill, John Lajoie, Garry Sleege
University of New Mexico	Muon Trigger	Doug Fields
Riken-BNL Research Center	Muon Trigger	Wei Xie, Gerry Bunce
University of Tennessee	Muon Trigger	Ken Read, Vasily Dzhordzahdze
Foreign Institutions		
Kyoto University	Muon Trigger	Kazuya Aoki, Naohito Saito, Hiroki Sato, Marcus Wagner
Moscow State University	Nosecone Calorimeter	Mikhail Merkin, Alexander Voronin
Riken (Japan)	Nosecone Calorimeter	Atsushi Taketani
INFN Triest	Nosecone Calorimeter	Andrea Vacchi

Table 3.1 Collaborating Institutions and Interests

4. Cost and Schedule

Section 5 of the PHENIIX forward upgrade letter of intent contains a rough estimate of costs for the muon trigger upgrade and the nosecone calorimeter upgrade. In addition we provide in the letter of intent a schedule for the implementation of the upgrade. Here we summarize that we estimate the costs for the muon trigger based on RPC technology including the cost for front-end and trigger electronics to $1.1 Million and for the nosecone calorimeter to about $4.4 Million. These are the hardware costs only.

These very preliminary cost estimates are compiled under the assumption that the silicon sensors and readout units are produced by Russian industry, under the control of the Moscow State University PHENIX group.

4.1 Sources of Funding

The total hardware costs are estimated to be about $5.5M. We will be applying to NSF for an instrumentation grant with a consortium of universities including Colorado, Illinois, Iowa State University, New Mexico and UC Riverside for a total of about $2M. This funding will cover the muon trigger upgrade. For the nosecone calorimeter we rely on DOE funding and forgein funding sources.

Initial funding for R and D will be coming from a number sources as shown in the following table.

R and D Funding Sources		
Institution	Amount	Item
UC Riverside	90K	Engineering (Solin), Nose cone Calorimeter R and D (Moscow)
Illinois	120K	RLT, RPC R and D, NCC R and D
RBRC	?	RLT
Kyoto	150k	Mu Tr R and D
Total	360K	

Table 4.1 Funding for initial R&D

4.2 Schedule

We present a very rough schedule in the table. Because of the cost of the nosecone calorimeter, we have left the decision whether to instrument one or both muon arms to the future. The following schedule leaves room for the instrumentation of both arms. The major milestones are 1) to submit the proposal to the NSF in January 2005. 2) To have the one arm of the muon trigger complete and debugged, in preparation for the long pp run in 2007, 3) to have the muon trigger operational in both arms before the long 500 GeV pp run in 2009 4) to have one of the nose-cone calorimeters with SMD in place for Run 8 – the high luminosity Au-Au run for the study of the χ_c 5) and finally to have both calorimeters (with SMD's) in place for run 9, well ahead of the series of proton and deuteron-nucleus runs. Because of the possible effects of the nosecone calorimeter on the muon resolutions without the SMD, the schedule of installation is intentionally left flexible, either to install the calorimeter without the SMD prior to run 7, or to delay till run 8 when the first SMD is projected to be ready. A rough schedule is shown in the table.

PROPOSALS	
LOI to collaboration	May 2004
Presentation to PAC	Sep 2004
Proposal to NSF	Jan 2005
MUON TRIGGER	
Run 5 [SiSi 200 14 wks; pp 200 10wks]	Fall 2004
RLT Prototype	Jan 2005
mutrig prototype installation	June 2005
Run 6 [AuAu 63 19wks; pp 500 2wks]	Fall 2005
Muon trig first arm operational	Fall 2006
Run 7 [pp 200 22; pp 63 5]	Fall 2006
Muon trig second arm operational	Fall 2007
Run 8 [AuAu 200 19]	Fall 2007
Run 9 [pp 500 29]	Fall 2008
NOSECONE CALORIMETER	
Run 5 [SiSi 200 14wks; pp 200 10wks]	Fall 2004
Nosecone prototype operational	Fall 2005
Run 6 [AuAu 63 19wks; pp 500 2wks]	Fall 2005
SMD prototype operational	Fall 20/06
Run 7 [pp 200 22wks; pp 63 5wks]	Fall 2006
Nosecone 1 SMD 1 operational	Fall 2007
Run 8 [AuAu 200 19wks]	Fall 2007
Nosecone 2 SMD 2 operational	Fall 2008
Run 9 [pp 500 29wks]	Fall 2008
Run 10 [dAu 63 29wks]	Fall 2009

Table 4.2 Schedule